pH Regulation in Human Sperm

Dissertation

zur

Erlangung des Doktorgrades (Dr. rer. nat.)

der

Mathematisch-Naturwissenschaftlichen Fakultät

der

Rheinischen Friedrich-Wilhelms-Universität Bonn

vorgelegt von

Elena Grahn

aus

Kirchen

Bonn 2023

Angefertigt mit Genehmigung der Mathematisch-Naturwissenschaftlichen Fakultät
der Rheinischen Friedrich-Wilhelms-Universität Bonn

1. Gutachter: Prof. Dr. U. Benjamin Kaupp

2. Gutachter: Prof. Dr. Michael Famulok

3. Gutachter: Prof. Dr. Michael Pankratz

4. Gutachterin: Prof. Dr. Dagmar Wachten

Tag der Promotion: 14.12.2023

Erscheinungsjahr: 2024

Summary

In the female reproductive tract, sperm undergo a maturation process, called capacitation, which enables sperm to fertilize the oocyte. The complex cellular mechanisms underlying capacitation are not well understood. Besides other cellular events, the sperm cytosol alkalizes and the intracellular calcium concentration rises, which changes the flagellar beating. Remarkably, during their journey through the female reproductive tract, human sperm face drastic changes in the extracellular pH (pH_o): in the vagina, pH_o is below 5; in the oviduct, at the site of fertilization, pH_o is above 7.5. Signaling cascades that regulate sperm swimming depend on the intracellular pH (pH_i): a rise in the cAMP concentration in sperm increases the flagellar beat frequency. cAMP, in turn, is produced by a HCO_3^--activated, soluble adenylyl cyclase, thus connecting its activity to pH_i via the $CO_2/HCO_3^-/H^+$ equilibrium. In addition, the sperm-specific, alkaline-activated calcium channel CatSper allows calcium influx that is crucial for a particular flagellar beating called hyperactivation. It has been suggested that changes in pH_o translate to changes in pH_i via transmembrane channels or exchangers. Several anion exchangers of the SLC family and CFTR were suggested to propagate an HCO_3^- influx, while sperm-specific Na^+/H^+ exchangers and Hv1 were suggested to facilitate proton extrusion.

In my thesis, I used electrophysiological, fluorometric, and pharmacological methods to decipher the cellular mechanisms that regulate pH_i in human sperm. I showed that upon extracellular alkalization, mimicking the increasing pH_o in the female reproductive tract, pH_i slowly follows pH_o. The pH_i is set by an amiloride-sensitive Na^+/H^+ exchange. Exposing sperm to physiological CO_2/HCO_3^- concentrations leads to rapid and persistent acidification caused by CO_2 diffusion into the cell and subsequent hydration to $HCO_3^- + H^+$ by carbonic anhydrase; HCO_3^- in turn activates the sAC. In contrast, HCO_3^- transport into the cell seems to play if any only a minor role in pH_i regulation. Thus, CO_2 diffusion over the membrane dominates over HCO_3^- transport. Further, I show that Hv1 is the only voltage-dependent pH regulator in human sperm. Using patch-clamp fluorometry, I was able to record the intracellular alkalization induced by depolarizing Hv1 currents, which were potentiated in presence of CO_2/HCO_3^-. Alkalization by Hv1 is, however, only transiently present for the duration of the depolarization. My results are corroborated by a recently assembled sperm

proteome, which also suggests that fewer proteins than previously thought are involved in pH regulation in human sperm.

Zusammenfassung

Auf dem Weg durch den weiblichen Reproduktionstrakt durchlaufen Spermien einen Reifungsprozess, die sogenannte Kapazitation. Erst im Laufe der Kapazitation erlangen Spermien die Fähigkeit zur Befruchtung der Eizelle. Die zugrundeliegenden zellulären Mechanismen sind nur teilweise verstanden. Unter anderem finden während der Kapazitation eine intrazelluläre Alkalisierung und ein Anstieg der intrazellulären Kalziumkonzentration statt, die eine Veränderung des Flagellenschlags verursachen. Auffallend ist, dass Spermien im weiblichen Reproduktionstrakt drastischen Veränderungen des äußeren pHs (pH_o) ausgesetzt sind: in der Vagina ist der pH-Wert von unter 5 sehr niedrig, wohingegen im Ovidukt, wo die Befruchtung stattfindet, ein pH-Wert von über 7.5 erreicht werden kann. Die Signalkaskade, die den Flagellenschlag und die Fortbewegung der Spermien reguliert, ist abhängig vom intrazellulären pH (pH_i): ein Anstieg der intrazellulären cAMP-Konzentration führt zu einer Erhöhung der Flagellenschlagfrequenz. cAMP wiederum wird von einer HCO_3^--aktivierten löslichen Adenylatcyclase produziert, deren Aktivität an das $CO_2/HCO_3^-/H^+$ Gleichgewicht geknüpft ist. Zusätzlich öffnet der Spermien-spezifische Kationenkanal CatSper, der für den entscheidenden Kalziumeinstrom zur Hyperaktivierung verantwortlich ist, bei intrazellulärer Alkalisierung. Transmembranproteine können Veränderungen des pH_o nach intrazellulär übertragen und den pH_i ändern. Spermien-spezifische Na^+/H^+-Austauscher und der Protonenkanal Hv1 könnten einen Protonenausstrom und damit eine intrazelluläre Alkalisierung bewirken. Es wurde zudem vermutet, dass Anionenaustauscher der SLC Familie, sowie der CFTR-Kanal, HCO_3^- leiten und so für einen Einstrom sorgen und damit das $CO_2/HCO_3^-/H^+$ Gleichgewicht verschieben könnten.

In meiner Arbeit habe ich elektrophysiologische, fluorometrische und pharmakologische Methoden angewendet, um die zellulären Mechanismen zu entschlüsseln, die den pH_i menschlicher Spermien regulieren. Ich konnte zeigen, dass nach einer extrazellulären Alkalisierung der pH_i dem pH_o folgt; diese intrazelluläre Alkalisierung wird durch einen Amilorid-sensitiven Na^+/H^+-Austauscher vermittelt. Setzt man Spermien physiologischen CO_2/HCO_3^--Konzentrationen aus, führt dies zu einer schnellen Ansäuerung, bedingt durch die CO_2 Diffusion über die Membran und die intrazelluläre Hydration zu $HCO_3^- + H^+$ durch die Carboanhydrase. Im Gegensatz dazu spielt ein potentieller HCO_3^--Einstrom über Transporter oder Austauscher bei der

pH Regulierung keine messbare Rolle. Des Weiteren konnte ich zeigen, dass Hv1 der einzige spannungsgesteuerte pH-Regulator in menschlichen Spermien ist. Mithilfe der Patch-Clamp Fluorometrie konnte ich zeigen, dass eine Depolarisation eine intrazelluläre Alkalisierung durch Hv1 hervorruft, welche in Anwesenheit von CO_2/HCO_3^- potenziert wird. Die durch Hv1 ausgelöste Alkalisierung war jedoch transient und hielt nur während der Depolarisation an. Meine Ergebnisse werden von einem kürzlich erstellten Proteom menschlicher Spermien untermauert, welches darauf schließen lässt, dass deutlich weniger Proteine als bislang vermutet in die pH-Regulation menschlicher Spermien involviert sind.

TABLE OF CONTENTS

List of abbreviations

A	Ampere
AE	anion exchanger
ANG-2	Asante NaTRIUM Green-2
bPAC	photoactivated adenylyl cyclase
BSA	bovine serum albumine
BTR1	bicarbonate-transporter-related protein 1
CA	carbonic anhydrase
cAMP	cyclic adenosine monophosphate
CatSper	cation channel of sperm
CFTR	cystic fibrosis conductance regulator
CHO	chinese hamster ovary
CNBD	cyclic nucleotide binding domain
DIDS	4,4′-diisothiocyano-2,2′-stilbenedisulfonic acid
EIPA	5-(N-ethyl-N-isopropyl)-amiloride
ENaC	epithelial sodium channel
ES	extracellular solution
HEK	human embryonic kidney
HSA	human serum albumin
HTF	human tubular fluid
I	current
ICC	immune cyto chemistry
IS	intracellular solution
KO	knock-out
M	molar
NBC	sodium bicarbonate cotransporter
NHA	sodium proton antiporter
NHE	sodium proton exchanger
NMDG	N-methyl-D-glucamine
PCF	patch-clamp fluorometry
pCO_2	CO2 partial pressure
PDE	phosphodiesterase

pH	negative logarithm of proton concentration
pH_i	intracellular pH
pH_o	extracellular pH
PKA	proteine kinase A
pPKA	phosphorylation by PKA
pY	tyrosine phosphorylation
R_a	access resistance
RT	room temperature
s.d.	standard deviation
sAC	soluble adenylyl cyclase
SLC	solute carrier
$t_{1/2}$	half-time constant
TAT1	testis-anion-transporter 1
V	volt
VSD	voltage-sensitive domain
wt	wild type
ZP	zona pellucida
°C	degree Celsius
µM	micro molar
τ	time constant tau
Ω	Ohm

1. Introduction

1.1 Fertilization in mammals

The fusion of the male and female gamete, sperm and oocyte, gives rise to new life. To this end, a single sperm cell needs to reach the oocyte, which is released into the oviduct. Millions of sperm are produced in the testis and stored in the epididymis; upon ejaculation sperm are mixed with the fluids of the male accessory glands and finally with the vaginal fluids (Samanta et al., 2018). At this point, sperm are motile but not yet able to fertilize the egg. For the successful fertilization, sperm have to swim through the cervix into the uterus and into the oviduct (Figure 1).

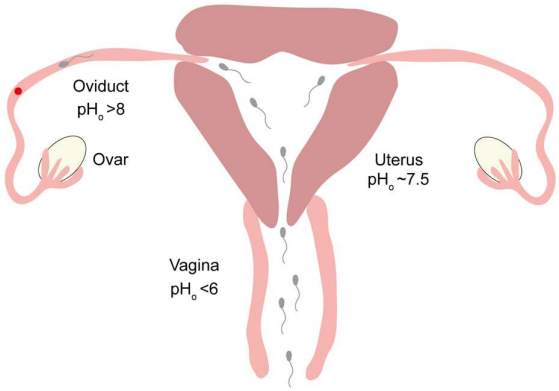

Figure 1. Scheme of the female reproductive tract and the travel route for sperm from point of ejaculation (vagina) to point of fertilization (oviduct) with respective pH_o. Red: oocyte.

The passage through the female reproductive tract not only selects sperm but also initiates a final maturation process (reviewed by Suarez & Pacey, 2006). Evidence for a maturation process in mammals was already reported almost 70 years ago. Rabbits were treated with pituitary gland extract to artificially induce ovulation. Sperm were placed in the oviduct at several time points before and after calculated ovulation occurred, and eggs were recovered after 36-42 hours to check for successful fertilization. No fertilized ova were found in rabbits that had been injected with sperm after or during ovulation. Sperm injection 5-7 hours before ovulation resulted in the highest rate of fertilized eggs (Austin, 1951; Chang, 1951). The authors proposed that sperm undergo physiological changes while being exposed to the chemical environment of the female reproductive tract and, thereby, gain the capacity to fertilize, which was later called “capacitation”. In the following decades, various physiological changes were observed that occur during the capacitation process: a

change in flagellar beating, called hyperactivation, an exocytotic release of hydrolytic enzymes, the acrosome reaction, activation of protein kinase A (PKA) by cyclic adenosine monophosphate (cAMP), and tyrosine phosphorylation (pY) by a tyrosine kinase (reviewed by De Jonge, 2017; Puga Molina et al., 2018a). However, despite much research for decades, the molecular mechanisms involved and the underlying time course of events during capacitation are still ill-defined. Nevertheless, several ingredients of the vaginal and uterine fluids were identified to be necessary for *in-vitro* capacitation: Albumin in the vaginal fluid removes cholesterol from the sperm's membrane and changes its biophysical properties (Flesch et al., 2001; Harrison and Gadella, 2005). Bicarbonate, HCO_3^-, activates the atypical soluble adenylyl cyclase (sAC) and induces cAMP production (Chen et al., 2000). Subsequently, cAMP triggers phosphorylation of proteins by PKA (pPKA; (Battistone et al., 2013; Leclerc et al., 1996; Visconti et al., 1995). Whereas a rise of cAMP and activation of PKA occur within the first minute of HCO_3^- exposure, pY is hardly detectable after one hour and completed after six hours of incubation (Battistone et al., 2013; Mukherjee et al., 2016). Opening of the calcium channel CatSper and the potassium channel Slo3 leads to calcium increase and hyperpolarization, respectively (Brown et al., 2016; Linares-Hernández et al., 1998; Patrat et al., 2002; Santi et al., 2010; Zeng et al., 2013). Elevated Ca^{2+} and HCO_3^- levels promote hyperactive flagellar beating, which is necessary for sperm to penetrate the vestment surrounding the oocyte (Carlson et al., 2007; Florman et al., 2008; Wennemuth et al., 2003) and hyperpolarization limits the Ca^{2+} influx (Brenker et al., 2014). Furthermore, sperm reportedly alkalize during capacitation (Cross and Razy-Faulkner, 1997; López-González et al., 2014; Vredenburgh-Wilberg and Parrish, 1995; Zeng et al., 1996), which supports opening of the CatSper channel (Lishko et al., 2011; Strünker et al., 2011). Finally, the acrosome reaction is triggered and enzymes are released, which enables the fusion of the gametes (Arnoult et al., 1996; Balbach et al., 2020; Bleil and Wassarman, 1983; Cross et al., 1988; Florman et al., 2008). This is a complex process, and the sequence of events is not entirely clear. The individual steps of the entire capacitation complex were studied *in vitro* and might, therefore, differ from the events occurring *in vivo*.

On the journey through the female reproductive tract, sperm encounter drastic changes in the extracellular environment regarding pH and HCO_3^-. The proton concentration is high in testis (pH_o ~6.85) and vagina (pH_o<6), and strongly decreases

in the oviduct (pH_o>8; David et al., 1973; Eggert-Kruse et al., 1993; Levine & Marsh, 1971; Maas et al., 1977; MacDonald & Lumley, 1970; Owen & Katz, 1999; Vishwakarma, 1962; Wagner & Ottesen, 1982; reviewed by Ng et al., 2018;). The major extracellular pH buffer, besides proteins, is the CO_2/HCO_3^- buffer. CO_2 is hydrated by water, forming carbonic acid (H_2CO_3; Equation 1). This reaction is usually slow; in the body, the reaction can be sped up bidirectionally by a factor of $1.7*10^4$ by cytosolic or extracellular carbonic anhydrases (Khalifah and Silverman, 1991). Carbonic acid rapidly dissociates to HCO_3^- and H^+:

$$CO_2 + H_2O \leftrightarrow H_2CO_3 \leftrightarrow HCO_3^- + H^+$$

Equation 1. The CO_2/HCO_3^- equilibrium in aqueous solutions.

With simplifying assumptions (virtually unlimited abundance of H_2O, rapid dissociation of H_2CO_3, pH = -log([H^+])), one can derive the Henderson-Hasselbalch equation:

$$pH = pK_a + \log\frac{c(HCO_3^-)}{c(CO_2)}$$

Equation 2. Henderson-Hasselbalch equation for determination of pH from pK_a and intra- and extracellular concentrations of the respective ions.

where the dissociation constant K_a is written as pK_a = -log(K_a). Accordingly, HCO_3^- should be low in the more acidic testis and vagina (testis 6.7 mM HCO_3^- (rat testis; Levine & Marsh, 1971); no data available for vagina) and high in the more alkaline oviduct (20-80 mM; David et al., 1973; Levine & Marsh, 1971; Maas et al., 1977; Vishwakarma, 1962). The partial pressure of CO_2, pCO_2, and hence the concentration of physically dissolved CO_2, are well-regulated and roughly constant in essentially all tissues of the human body under physiological conditions with normal blood supply (Boron, 2016). H^+ and HCO_3^- are crucial for fertilization: intracellular alkalization promotes opening of CatSper and HCO_3^- activates sAC, which is the main cAMP source in human sperm (Ren et al., 2001; Chen et al., 2000; Hess et al., 2005; reviewed by Rahman et al., 2013). The concentration of the second messenger cAMP is a tug-of-war between synthesis via sAC and hydrolysis via a phosphodiesterase (PDE; Fisch et al., 1998; reviewed by Buffone et al., 2014). In addition, the cell is equipped with a variety

of proteins that have been implied to regulate pH directly or indirectly via transport of H^+ or HCO_3^-, respectively.

1.2 The pH & HCO_3^- regulation in sperm

It has been proposed that sperm are equipped with several transmembrane proteins that transport H^+ or HCO_3^- across the membrane. The proteins represent either ion channels or solute carriers (SLC; Figure 2). The cystic fibrosis conductance regulator, CFTR a channel, and two different types of the solute carrier family, SLC4 and SLC26, are suggested to transport HCO_3^- into the cell and thereby activate sAC. H^+ is thought to leave (or enter) sperm via exchange for Na^+ by sNHE or NHA, or via the voltage-gated proton channel Hv1. The exchangers and Hv1 have been implied in alkalization of sperm during capacitation. Additionally, sperm express carbonic anhydrase isoforms CAII and CAIV, which catalyze the chemical reaction $CO_2 + H_2O \leftrightarrow HCO_3^- + H^+$. CAII is located intra- and CAIV extracellularly (Wandernoth et al., 2015, 2010).

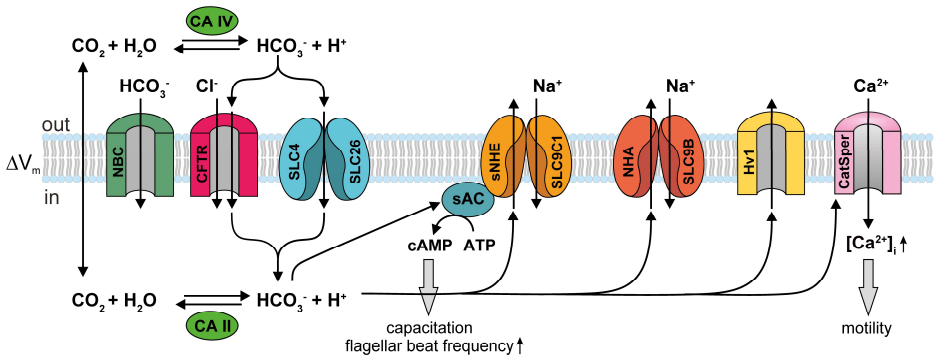

Figure 2. Putative pH-regulating proteins in human sperm. CA, carbonic anhydrase II and IV; NBC, sodium-dependent bicarbonate channel; CFTR, cystic fibrosis transmembrane regulator; SLC4 and SLC26, solute carrier families 4 and 26 which transport bicarbonate and anions; sNHE, sperm-specific sodium/hydrogen exchanger SLC9C1; sAC, soluble adenylate cyclase; NHA, sodium/hydrogen antiporters of the SLC9B family; Hv1, voltage-gated proton channel; CatSper, sperm-specific cation channel.

Some proteins shown in Figure 2 and their putative functions have been investigated in great detail, whereas the presence and role of others have only been examined cursorily. Finally, for some of these proteins it remains unclear whether they are important for function of mature sperm or for spermatogenesis. Their function in human sperm has been inferred largely from experiments in other species. In the following, I will introduce these signaling proteins and events in greater detail.

CFTR is a Cl^- channel associated with the genetic disorder cystic fibrosis that is characterized by a disturbed ion composition of some body fluids, notably fluids of the respiratory tract (reviewed by Mall & Hartl, 2014). CFTR can transport both Cl^- and HCO_3^-; the permeability ratio $Cl^-:HCO_3^-$ = 4:1 (Tang et al., 2009). Male and female patients are sub- or infertile (Schulz et al., 2006; reviewed be Ahmad et al., 2013). In 95% of male cystic fibrosis patients, an anatomical defect – the congenital bilateral absence of the *vas deferens* – leads to infertility but nonetheless they produce sperm and can have children with the help of *in vitro* reproductive techniques (reviewed by de Souza et al., 2017). In human sperm, the protein was detected via immunocytochemistry (ICC) in the equatorial segment of the head, but not in the flagellum (Xu et al., 2007). Treating sperm during capacitation with the blocker CFTR inhibitor-172 ($CFTR_{inh}$-172), reduced the cAMP increase, the amount of hyperactivated sperm, the amount of pY and pPKA, and the hyperpolarization that was observed in absence of the drug (Li et al., 2010; Puga Molina et al., 2017). In addition, sperm acidified during inhibition of CFTR but an explanation for this observation seems missing (Puga Molina et al., 2017). In mouse sperm, inhibition of CFTR reduced the acrosome reaction, intracellular alkalization, cAMP production, and hyperpolarization during capacitation (Hernández-González et al., 2007; Xu et al., 2007).

SLC4 is a diverse family of HCO_3^-/Cl^-/anion exchangers (AE) and Na^+-coupled transporters. The most prominent member of the family is SLC4A1, also known as Band-III protein, which extrudes HCO_3^- from erythrocytes (review by Romero et al., 2013). A Band-III-related protein was detected in the equatorial segment of human sperm via ICC (Parkkila et al., 1993) and SLC4A11, human bicarbonate-transporter-related protein (BTR1), was found in human testis via Gene Bank search and Northern blotting (Parker et al., 2001). Furthermore, another member of the SLC4A family, the sodium-dependent electrogenic HCO_3^- transporter (Na$^+$/bicarbonate cotransporter, NBC) was suggested to be responsible for the initial HCO_3^- influx and accompanying membrane hyperpolarization (Demarco et al., 2003; Puga Molina et al., 2018b). Tyrosine phosphorylation and hyperpolarization was decreased under Na^+-free capacitating conditions and in presence of the NBC inhibitor S0859 (Puga Molina et al., 2018b).

Several Cl^-/HCO_3^- exchangers of the SLC26 family of anion exchangers were suggested to contribute to $HCO3^-$ transport in sperm or sperm maturation. Male infertility was

reported in patients with congenital chloride diarrhea, a genetic disease caused by a mutation in the SLC26A3 gene (Hihnala et al., 2006a; Höglund et al., 2006). In humans, the protein was only detected in developing spermatids, but not in fully developed spermatozoa (Hihnala et al., 2006b), whereas in guinea pig sperm, SLC26A3 was detected in the acrosomal region (Chen et al., 2009) and in mouse sperm, the protein was shown to be located in the midpiece (Chávez et al., 2012). SLC26A3$^{-/-}$ mice show reduced sperm count with abnormal morphology, reduced motility, and impaired capacitation (El Khouri et al., 2018). The anion transporter SLC26A8, testis-anion-transporter (TAT1), of the SLC26 family was suggested to participate in HCO_3^- transport. Transcripts were detected in spermatids by *in-situ* hybridization, and the protein was localized in the equatorial segment and annulus by ICC (Rode et al., 2012; Touré et al., 2001). Cells heterologously co-expressing TAT1 and CFTR showed enhanced CFTR currents and sulfate transport sensitive to the anion exchange inhibitor 4,4′-Diisothiocyano-2,2′-stilbenedisulfonic acid (DIDS), suggesting an interaction of both proteins (Rode et al., 2012; Touré et al., 2001). In men, three heterozygous missense mutations were identified that cause asthenozoospermia (Dirami et al., 2013) and KO-mice are sterile (Touré et al., 2007).

Evidence for Na^+-dependent pH regulation was found in capacitated human sperm which were reported to have a lower pH_i after incubation in Na^+-free medium (Garcia and Meizel, 1996). The lower pH_i recovered in presence of Na^+; the recovery was inhibited by 5-(N-ethyl-N-isopropyl)-amiloride (EIPA), an inhibitor of Na^+/H^+ exchangers (Garcia and Meizel, 1999). Human sperm are equipped with three different potential Na^+/H^+ exchangers. Two testis-specific Na^+/H^+ antiporters, SLC9B1 & 2 (NHA1 & 2), are reportedly expressed in the principal piece of human sperm and might exchange Na^+ for H^+ like the Na^+/H^+ exchangers of the SLC9A family, which are widely expressed throughout the human body (S. R. Chen et al., 2016; Ye et al., 2006; reviewed by Pedersen & Counillon, 2019). NHA1 was cloned from human testis tissue (Ye et al., 2006). In mouse sperm, *zona pellucida* (ZP) proteins evoke a pH_i increase, which is mediated by NHA1 (Balbach et al., 2020). A sperm-specific Na^+/H^+ exchanger, SLC9C1 (sNHE), was detected in mouse and also predicted for human sperm (Wang et al., 2003). SLC9C1$^{-/-}$ mice were infertile despite normal sperm count. Sperm were immotile due to reduced sAC activity and decreased cAMP content (Wang et al., 2007). This defect is partially rescued with membrane-permeable cAMP analogues, the

optogenetic tool bPAC that synthesizes cAMP, or intracellular alkalization with NH_4Cl (Jansen et al., 2015; Wang et al., 2007, 2003). sAC and sNHE were proposed to associate with each other, which could explain the motility defects induced by the low cAMP content and synthesis (Wang et al., 2007, 2003). Heterologous expression of the human protein was not successful and no functional evidence of sNHE in human sperm could be shown so far. Recently, our research group showed that the sea urchin sNHE is a voltage-gated Na^+/H^+ exchanger (Windler et al., 2018). The homologous protein consists of three functional domains: 1) an exchanger domain, that exchanges 1 Na^+ for 1 H^+, 2) a voltage-sensor domain (VSD) with 7 positively charged amino acids, that activates the exchanger domain upon hyperpolarization, and 3) a C-terminal cyclic nucleotide-binding domain (CNBD), which alters the exchange activity upon cAMP binding. The protein sequences of human and mouse, however, lack certain amino-acid residues known to be important for Na^+/H^+ exchange, voltage sensing, and cAMP binding of the CNBD (Windler et al., 2018).

Human sperm are equipped with another voltage-gated pH regulator: the proton channel Hv1. Its peculiar architecture and its high selectivity for protons is exceptional (Ramsey et al., 2006; Sasaki et al., 2006). Unlike classic voltage-gated ion channels, Hv1 contains no prototypical pore domain; instead, the VSD acts as a pore for protons. Hv1 opens upon depolarization, but is strongly dependent on the pH difference across the membrane (Cherny et al., 1995). Hv1Sper, a sperm-specific isoform that lacks the first 68 amino acids, senses the absolute pH and its gating is shifted to more positive potentials at more alkaline pH (Berger et al., 2017). In human sperm, proton currents that increase after capacitation, can be recorded by the patch-clamp technique (Lishko et al., 2010). It was hypothesized that Hv1 might be responsible for the slow alkalization during capacitation (Lishko et al., 2010). However, the positive V_m required to open Hv1 are unlikely to exist in sperm. Moreover, it is unclear how the channel can alkalize sperm during capacitation when supposedly cells hyperpolarize (Florman et al., 2010). Thus, the physiological role of Hv1 remains enigmatic. Interestingly, Hv1 currents can be inhibited by zinc (Ramsey et al., 2006), an ion that is present in the low millimolar range in the seminal fluid (Owen and Katz, 2005). Possibly, zinc will be scavenged by albumin in the female reproductive tract (Lu et al., 2008; Raffi et al., 1977; Tjokronegoro and Sirisinha, 1975).

Several research groups used mass spectrometry to determine the proteome of human sperm (Amaral et al., 2014; Baker et al., 2013; Gu et al., 2011; Wang et al., 2013). Expression of several of the proteins that are putatively involved in pH regulation was confirmed (Table 1). However, there are also discrepancies between the protein data sets: none of the four different proteome data sets contains all of the pH-regulating proteins. Except for NHA1&2 (SLC9B1&2), all of them are detected in at least one of the proteomes. This leaves room for doubts and demands further validation of the proteomic data and independent functional evidence.

Table 1. Putatively pH-regulating proteins validated by mass spectrometry.

Protein	Wang et al., 2013	Baker et al., 2013	Amaral et al., 2014	Gu et al., 2011
CA II	✓			
CA IV	✓		✓	
CFTR				✓
SLC4A1 (AE1)	✓			
SLC4A3 (AE3)				✓
SLC4A5 (NBC)				✓
SLC26A8 (TAT1)	✓		✓	
SLC9A1 (NHE1)	✓			
SLC9A2 (NHE2)				✓
SLC9A3 (NHE3)		✓		
SLC9A5 (NHE5)				✓
SLC9A9 (NHE9)				✓
SLC9B1 (NHA1)				
SLC9B2 (NHA2)				
SLC9C1 (sNHE1)	✓			
SLC9C2 (sNHE2)				
HVCN1 (Hv1)	✓			

✓ = detected in mass spectrometric analysis.

1.3 How conserved is sperm signaling among species?

Many studies on capacitation using mouse, rabbit, or bull sperm served as blueprint to draw also conclusions for human sperm. One difference between most experimental studies on human sperm versus sperm from other species is the fact that sperm of

other species are in most cases extracted from epididymis. Human sperm samples, in contrast, are mostly purified from the ejaculate. During ejaculation, sperm are mixed with fluids of the accessory sex glands. Exposure to seminal fluid is a step of the maturation process of sperm for the upcoming fertilization; a step which is often omitted in studies of other species and might, thereby, lead to different experimental results.

Moreover, although sperm of different species express a similar set of homologous proteins, the proteins often differ in their functional properties, which changes the entire signaling pathway. For these reasons, it has been cautioned to generalize conclusions drawn from a single species (reviewed by Kaupp & Strünker, 2017). For example, human and mouse sperm both functionally express CatSper and Slo3. However, in human sperm, CatSper can be opened by nanomolar concentrations of progesterone and prostaglandins (Kirichok et al., 2006; Lishko et al., 2011; Strünker et al., 2011), whereas the murine CatSper is insensitive to physiological concentrations of progesterone and prostaglandins (Lishko et al., 2011). Slo3, the inward-rectifying potassium channel which determines V_m and, thereby, indirectly controls voltage-gated channels, is strongly activated by Ca^{2+} but only slightly sensitive to pH_i in human sperm (Brenker et al., 2014). In contrast, Slo3 is insensitive to Ca^{2+} but strongly dependent on pH_i in mouse sperm (Navarro et al., 2007). Another difference is the expression of Hv1 in human but not in mouse sperm (Lishko et al., 2010). Thus, the study of pH regulation in other sperm species might provide only limited insight into the pH regulation of human sperm. Therefore, pH regulation should be studied in human sperm directly.

1.4 Aim

The aim of my PhD Thesis was to identify the mechanisms of pH_i and HCO_3^- regulation in human sperm. To this end, I used single-cell fluorometry to record pH_i, $[Na^+]_i$ and $[Ca^{2+}]_i$ and established patch-clamp pH-fluorometry on human sperm to investigate voltage-dependent pH_i regulation.

2. Materials & Methods

2.1 Cell systems and preparation

2.1.1 Sperm cells

Human semen samples were donated by healthy adult males with their prior written consent and the approval of the ethic committee of the University of Bonn (042/17). Ejaculates were liquefied at room temperature (RT) for 30-60 min and purified by the "swim-up" procedure (Strünker et al., 2011) in human tubular fluid (HTF) medium. After 30-45 min, the supernatant, containing motile sperm, was collected, centrifuged at 700xg for 10 min and resuspended in fresh HTF. Samples were stored in HTF at 37°C diluted to $1*10^7$ cells/ml until they were further prepared for recordings.

Table 2. Composition of human tubular fluid (HTF) for preparation of human sperm.

HTF	
NaCl	93.8 mM
Na-lactate	21.4 mM
HEPES	21 mM
KCl	4.69 mM
$NaHCO_3$	4 mM
D-glucose	2.78 mM
$CaCl_2$	2.04 mM
Na-pyruvate	0.33 mM
$MgSO_4$	0.2 mM
KH_2PO_4	0.37 mM

pH adjusted to 7.35 with NaOH (continuously bubbled with 95%O_2/5% CO_2)

Mouse sperm were obtained from C57Bl/6N WT or sNHE-KO mice that were anaesthetized with isoflurane (Abbvie, Ludwigshafen, Germany) and killed by cervical dislocation according to the German law of animal protection and the district veterinary office. For mouse sperm preparation, cauda and corpus epididymis were extracted through a small abdominal incision and separated from fat. The tissue was incised several times and transferred to TYH buffer for the "swim-up" procedure. After 15 min, sperm were collected from the supernatant, centrifuged at 700xg for 10 min and resuspended in fresh TYH medium. Sperm were diluted to $1*10^7$ cells/ml in TYH

medium and stored at 37°C until further processed. sNHE-KO mice were purchased from the Jackson Laboratory (B6; 129S6-Slc9a10tm1Gar/J, stock number: 007661).

Table 3. Composition of TYH buffer for preparation of mouse sperm.

TYH buffer	
NaCl	138 mM
Na-lactate	10 mM
HEPES	10 mM
D-glucose	5.6 mM
KCl	4.8 mM
$CaCl_2$	2 mM
KH_2PO_4	1.2 mM
$MgSO_4$	1 mM
Na-pyruvate	0.5 mM

pH adjusted to 7.4 with NaOH

For fluorometric and electrophysiological recordings, human and mouse sperm ($1*10^7$ cells/ml) were mixed with 3 mg/ml human serum albumin (HSA) or bovine serum albumin (BSA), respectively. The cells were then pipetted on poly-L-lysine (PLL) coated coverslips submerged in ES. 10 minutes after this step, the recordings were started.

2.1.2 Chinese hamster ovary (CHO) cells

The immortalized CHO cell line, CHO-K1 (further labelled CHO) was used. For some experiments, a CHO-K1 cell line stable expressing hHv1 was used (further labelled CHO-hHv1). The preparation of the hHv1-expressing cell line was performed and kindly provided by Dr. W. Bönigk and Dr. H. Körschen. All CHO cell lines were kept in DMEM/F-12 medium (Life Technologies, Carlsbad, USA) + 10% FCS at 37°C (5% CO_2). For fluorometrical and electrophysiological experiments, cells were grown on PLL-coated 5 mm cover slips with 60% confluency.

2.1.3 Human embryonic kidney (HEK) cells

The immortalized HEK-293 cell line was kept in DMEM-medium (Life Technologies, Carlsbad, USA) + 10% FCS at 37°C (5% CO_2). For fluorometrical and electrophysiological experiments, cells were grown on PLL-coated 5 mm cover slips with 60% confluency.

2.2 Chemicals and solutions

All chemicals and inhibitors were purchased from Carl Roth (Karlsruhe, Germany), Sigma Aldrich (St. Louis, MO), or Thermo Fisher Scientific (Waltham, MA) if not stated otherwise. ADCY10 inhibitor #8164 was kindly donated by Dr. J. Buck.

Table 4. Composition of extracellular solution (ES) for electrophysiological and fluorometrical recordings.

Extracellular solution (ES)	
NaCl	140 mM
Mannitol	10 mM
KCl	5.4 mM
HEPES	5 mM
$CaCl_2$	1.8 mM
$MgCl_2$	1 mM
pH adjusted to 7.35 with NaOH	

Table 5. Composition of ES with 15 mM NH_4Cl for acid-load experiments.

ES with NH_4Cl	
NaCl	125 mM
NH_4Cl	15
Mannitol	10 mM
KCl	5.4 mM
HEPES	5 mM
$CaCl_2$	1.8 mM
$MgCl_2$	1 mM
pH adjusted to 7.35 with NaOH	

Table 6. Composition of Na^+-free ES (ES-NMDG; Na^+ substituted with NMDG).

ES with NMDG	
NMGD-OH	140 mM
Mannitol	10 mM
KCl	5.4 mM
HEPES	5 mM
$CaCl_2$	1.8 mM
$MgCl_2$	1 mM

pH adjusted to 7.35 with HCl

Table 7. Composition of pH-calibration solutions.

High K^+ pH-calibration solutions			
	pH 5.5/6.5	pH 7.5	pH 8.5
KCl	135 mM	135 mM	135 mM
MES	20 mM		
HEPES		20 mM	
Tris			20 mM
$CaCl_2$	1.8 mM	1.8 mM	1.8 mM
$MgCl_2$	1 mM	1 mM	1 mM
Nigericin	0.015 mM	0.015 mM	0.015 mM

pH adjusted to 5.5, 6.5, 7.5 or 8.5 with HCl or KOH

Table 8. Composition of the HCO_3^-/CO_2-containing extracellular solutions.

ES with CO_2/HCO_3^-			
	pH 7.35	pH 6.5	pH 7.5
NaCl	115 mM	137 mM	110 mM
$NaHCO_3$	25 mM	3 mM	30 mM
Mannitol	10 mM	10 mM	10 mM
KCl	5.4 mM	5.4 mM	5.4 mM
HEPES	5 mM	5 mM	5 mM
$CaCl_2$	1.8 mM	1.8 mM	1.8 mM
$MgCl_2$	1 mM	1 mM	1 mM

pH adjusted to 7.35, 6.5, 7.5 or 8.5 with NaOH (continuously bubbled with 95%O_2/5% CO_2)

Table 9.Composition of intracellular recording solutions (IS) for patch-clamp recordings.

Intracellular solutions (IS)		
	Human sperm, CHO	Mouse sperm
NMDG-OH	140 mM	
Aspartic acid		130 mM
Mg-ATP	4 mM	4 mM
NaCl	1.4 mM	1.4 mM
EGTA	1 mM	1 mM
MES	1 mM	1 mM

pH adjusted to 6.5 with methane sulfonate (human sperm, CHO) or Cs-OH (mouse sperm), osmolarity adjusted to 300 mOsm/l with mannitol

HCO_3^--containing solutions were bubbled with Carbogen (5% CO_2, 95% O_2) for at least 30 min before pH was adjusted. HCO_3^--containing solutions were continuously bubbled with Carbogen during experiments to maintain constant pCO_2 and pH. Prior to all recordings, the pH of all used solutions was checked with a calibrated pH-meter (SevenEasy, Mettler Toledo, Columbus, OH) and adjusted, if necessary. All extracellular solutions had osmolarities of 290-300 mOsm/l.

2.3 Experimental methods

2.3.1 Experimental setup

Electrophysiological and fluorometric recordings were performed on an inverted IX71 microscope (Olympus, Tokyo, Japan) equipped with a 60× water immersion objective and an additional 1.6x magnification lens for PCF. The Spectra Xlight engine (Lumencor, Beaverton, OR) LED lamp was used for excitation of fluorescent indicators. An EMCCD camera (iXon Ultra DU-897U, Andor Technology, Belfast, Ireland) controlled by the Andor Solis software (Andor Technology, Belfast, Ireland; version 4.30.30034.0) was used for imaging. The patch-clamp setup consisted of a pipette holder with an air-filled tube system and a headstage pre-amplifier (HEKA Elektronik GmbH, Lambrecht, Germany). The Axopatch 200B amplifier was connected to a Digidata 1440A acquisition board controlled by the software ClampEx (Molecular Devices, Union City, CA; version 10.2.0.15). Patch pipettes were pulled from borosilicate capillaries (Hilgenberg, Malsfeld, Germany) using a DMZ puller (Zeitz Instruments GmbH, Martinsried, Germany). Object table and pipette holder were controlled using a

micromanipulator (Scientifica, Uckfield, UK). All experiments were conducted at room temperature (20-23°C).

2.3.2 Fluorometry

2.3.2.1 Fluorescent indicators

For fluorometry, acetoxymethyl (AM)-esters of the indicators were used. The AM-esters of the molecules are uncharged and can permeate cell membranes. Once the molecule is inside of the cell, the AM-group is hydrolyzed by unspecific cellular esterases. Thereby, molecules are left with charged side groups and are "trapped" in the cell.

For recording changes of the intracellular pH, pHrodo-RED (Thermo Fisher Scientific, Waltham, MA) was used. The pH-sensitive molecule has a large dynamic range of pH 4-9 and a pKa of 6.5. Excitation and emission maxima are 560 nm and 585 nm, respectively. With increasing proton concentration and thereby lower pH, the pHrodo-RED fluorescence increases. For single-cell fluorometry, cells were loaded with 3.3 µM pHrodo-Red-AM for 12 min at 37°C, followed by centrifugation and washing. For PCF, 12.5 µM pHrodo-RED-maleimide was added to the IS before loading the pipette. Excitation and emission filters used were: 543/22 nm and 568LP nm, respectively.

Relative changes of the intracellular Ca^{2+}-concentration were recorded using CalBryte-520-AM (AAT Bioquest, Sunnyvale, CA). Excitation and emission maxima are at 493 nm and 515 nm. The fluorophore binds Ca^{2+}-ions with a K_D of 320 nM. The fluorescence intensity increases with increasing Ca^{2+}-binding. Sperm were loaded with 2 µM Calbryte-520-AM + 0.05% Pluronic F-127 for 60 min at 37°C, followed by one washing step. Excitation and emission filters used for fluorometry were 472/30 nm and 525/35 nm (Thorlabs, Newton, NJ), respectively.

Relative intracellular changes of the Na^+-concentration were recorded using Asante Natrium Green-2-AM (ANG-2, TEFLabs, Austin, TX). This Na^+-sensitive indicator can be excited with 488 nm and has an emission maximum at 548 nm (Lamy and Chatton, 2011). The emission intensity increases with increasing Na^+ concentrations. The K_D for Na^+ binding is 38.6 nM (Lamy and Chatton, 2011). Sperm were loaded with 10 µM ANG-2-AM + 0.05% Pluronic F-127 for 60 min, at 37°C, followed by one washing step. Excitation and emission filters used for fluorometry were 472/30 nm and 525/35 nm (Thorlabs, Newton, NJ), respectively.

2.3.2.2 Fluorometric recording

For fluorometric imaging, coverslip areas with non-overlapping cells were chosen. For recordings of sperm, cells with a freely and continuously beating flagellum were chosen. During all experiments, a continuous flow of perfusion was applied. Changes of extracellular solution were conducted manually at predefined time stamps during recording. A sampling rate of 1 or 2 Hz (0.5 Hz for Figure 15B) was used for imaging.

2.3.2.3 pH-calibration

To calibrate the pH retrospectively, the K^+/H^+-ionophore nigericin was used. The ionophore is inserted in the membrane and equilibrates intra- and extracellular $[H^+]$ and $[K^+]$ (Richard Chaillet and Boron, 1985). To this end, calibrations solutions (pH 5.5, 6.5, 7.5, or 8.5 + 0.015 mM nigericin) containing 135 mM K^+, which is close to the physiological $[K^+]_i$ of sperm, were successively washed in the bath after the recording (Figure 5). When sperm were exposed to the first nigericin-containing calibration solution, the fluorescence slowly changed, but reached a steady-state within 4-7 minutes. For the following calibration solutions, the fluorescence changed much quicker and reached a steady-state in <3 minutes. Because the whole calibration process took up to 15 min and the calibration solutions are non-physiological and harming for the cells, sperm frequently died during recording (running full or out of fluorophore) and could not be analyzed. The calibration, therefore could only be successfully performed following shorter initial experiments.

2.3.3 Electrophysiology

2.3.3.1 Patch-clamp technique

The patch-clamp technique allows to record ionic currents across cell membranes and is a powerful tool to investigate voltage-sensitive ion channels (Hamill et al., 1981; Sakman and Neher, 1984). For this method, the experimental setup consists of two microelectrodes: one measuring electrode in the patch pipette submersed in IS, and one reference electrode, submersed in a 3 M KCl agar-filled glass pipette in the bath chamber. The membrane potential (V_m) of the cell can be clamped to a desired command potential (V_c) by injecting a current (I) through the measuring electrode. By this, ionic currents across the membrane can be recorded. For this purpose, a clean, fire-polished glass pipette is brought in contact with an isolated cell and a seal with

high resistance (>1 Gigaohm, so-called "gigaseal") and mechanical stability can be formed between membrane and pipette (Hamill et al., 1981). The membrane patch in the pipette opening is electrically isolated from the extracellular medium and single-cell currents across this patch can be recorded. This configuration is called cell-attached mode (Figure 3, middle).

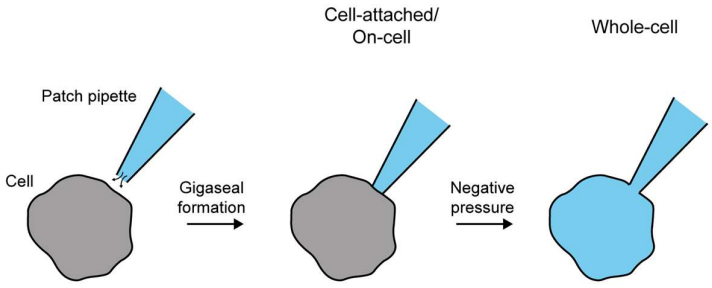

Figure 3. Establishing the whole-cell configuration for patch-clamp recording.

In my thesis, I used a variation of this technique. I recorded currents across large parts of the sperm membrane instead of a small membrane patch, in the so-called whole-cell configuration (Figure 3, right). To this end, a fire-polished glass patch pipette, filled with intracellular solution (Table 9) is brought to close contact with the membrane surface to form the gigaseal. Short pulses of negative pressure are used to disrupt the membrane patch in the pipette to obtain the whole-cell configuration. Consequently, the pipette electrode gains electrical access to the inside of the cell and the currents across large parts of the cell membrane can be recorded. The access resistance (R_a) between pipette and the inner cell is in the low MΩ range. Since the pipette volume is larger than the cytoplasm volume, the cytoplasm of the cell is replaced by the pipette solution.

2.3.3.2 Patch-clamp recordings

For patch-clamp recordings, cells with sufficient distance from other cells were selected. Motile sperm with only their head attached to the coverslip, a freely beating flagellum, and a visible cytoplasmic droplet were chosen. Initial resistance of the patch pipettes was 10-16 MΩ for sperm and 3-8 MΩ for HEK or CHO cells. Pipette offset and capacitance was compensated before sealing. After gigaseal formation, the whole-cell configuration was achieved by manually applying short pulses of negative pressure at a holding potential V_m = -30 mV. Whole-cell currents were sampled with 2 kHz. Before

and between recordings, cells were held at -30 mV. Cells were continuously perfused with extracellular solution.

2.3.3.3 Patch-clamp fluorometry (PCF)

Methods for the patch-clamp recordings equally apply for PCF recordings with some additions: During the break-in process, loading of cells with pHrodo-Red maleimide was observed with the EMCCD camera. Recordings were first started when the cell loading process reached a saturation. The half-time $t_{1/2}$ of filling sperm flagella with dye was ~50 s (Figure 8B) which is about tenfold slower than the reported filling time of mouse sperm with Lucifer Yellow (Kirichok et al., 2006). Images were acquired at 5 Hz.

2.4 Analysis

2.4.1 Analysis of electrophysiological data

Electrophysiological data was processed and analyzed with ClampFit (Molecular Devices, Union City, CA; version 10.0.3.03) and Igor Pro. Current traces were filtered using a boxcar filter (width 11 data points, i.e. 5.5 ms).

2.4.2 Analysis of imaging data

Images and movies were processed and analyzed with ImageJ. Motile sperm with only their head attached to the coverslip were chosen for analysis. ROIs were drawn by hand and the mean intensity of the chosen ROI was extracted and used for further analysis. ROIs of PCF recordings were restricted to around 10-15 µm in length, including the midpiece and the first part of the principle piece (Figure 8A). ROIs of fluorometric recordings were restricted to the sperm head, the midpiece, and up to the first quarter of the principle piece (Figure 4). These parts were little perturbed by flagellar beating. The rest of the sperm flagellum, beating at frequencies around 5 Hz (Schiffer et al., 2020), was excluded from analysis. Movies from PCF experiments were motion-corrected with the ImageJ plugin "MultiStackReg" to compensate for slow drifts of the patch pipette (less than 1 µm/min).

IgorPro (Wavemetrics, Portland, OR; version 6.3.7.2) was used for all further processing of the data. Fluorescence data are presented as $\Delta F/F$, with F as the initial fluorescence at the beginning of the recording (mean of the first 5 s). For some

experiments, pH signals were calibrated at the end of the recording in order to quantify changes in pH_i. To this end, the fluorescence at steady-state (mean of 5 s) after exposure to high-K^+/nigericin calibration solution with pH 8.5, 7.5, 6.5, and 5.5, was fitted with a sigmoid function and used to calculate pH_i for every single cell (Figure 5 shows an exemplary calibration curve with averaged data of 16 cells). PCF fluorescence traces from mouse and CHO cells were corrected for slow diffusion of the dye into the cell by subtraction of a mono-exponential fit. Fluorescence traces from ANG-2-loaded sperm were corrected for bleaching by subtraction of a mono-exponential fit. Time constants τ of fluorescent changes were determined by mono-exponential fitting. For complex kinetics, the half-time $t_{1/2}$ was used instead of τ. $t_{1/2}$ was defined as the time required for the in- or decrease of the process to reach 50% of the amplitude. To calculate the latency of the transient Ca^{2+} responses, the latency of the bath exchange measured with Alexa488 (wash-in = 3.1 ± 0.9 s, wash-out = 4.1 ± 3.6 s; n = 4) was subtracted from the latency of the Ca^{2+} responses.

3. Results

3.1 pH_i regulation via Na^+/H^+ exchange and the Hv1 proton channel

3.1.1 Single-cell fluorometry

To decipher the complex pH_i regulation in human sperm, I recorded single sperm using the pH fluorometry technique. I loaded sperm with a pH-sensitive dye (Figure 4). The cells were pipetted onto PLL-coated cover slips so that sperm head was attached to the surface; the flagellum was still free to beat. An intact head and flagellum and a steady, regular flagellar beat were used as selection criteria for analysis.

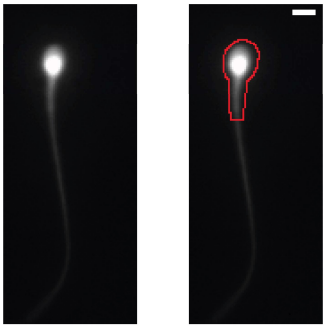

Figure 4. Single-cell pH fluorometry. Fluorescence microscopy of a human sperm cell loaded with the pH indicator pHrodo-Red AM. Right: the red marking shows the manually chosen region of interest (ROI) for the analysis. Scale bar: 3.5 µm.

Preliminary experiments with the ratiometric pH indicator 2',7'-Bis-(2-carboxyethyl)-5-(and-6)-carboxyfluorescein acetoxymethylester (BCECF-AM) gave only modest results: After brief light exposure, the flagellar beat of BCECF-loaded sperm stopped abruptly, suggesting that BCECF-loaded sperm got damaged during light exposure. Indeed, BCECF is notorious for photo-damage at high, continuous light intensities (Nishigaki et al., 2006). Therefore, I switched to the relatively novel pH indicator pHrodo-Red. pHrodo-Red AM-loaded sperm cells were viable for >45 min under continuous light exposure while photo-bleaching was negligible. To determine pH_i, sperm membranes were made permeable to protons with the K^+/H^+ ionophore nigericin. When added to cells, the ionophore is inserted into the plasma membrane and pH_i and pH_o quickly equilibrate. Calibration solutions with different pH_o (pH 5.5, 6.5, 7.5, 8.5) were then washed-in and the change in fluorescence of the sperm was continuously recorded. The steady-state fluorescence at the different pH_o was used to fit a calibration curve and the pH_i of the single cells was calculated in retrospect (Figure 5). Cells kept in physiological ES (pH 7.35) had an initial $pH_i = 7.25 \pm 0.4$

(mean ± s.d.; n_{exp} = 37; n_{cells} = 206). In conclusion, the pH indicator pHrodo-Red faithfully reports pH_i.

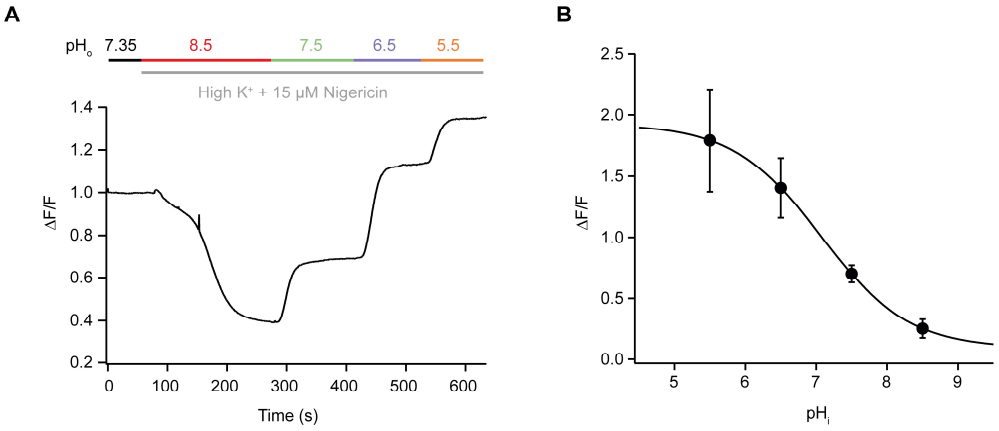

Figure 5. Nigericin-based pH calibration. (A) Calibration of pHrodo-Red with different K^+-based pH solutions in the presence of the K^+/H^+ ionophore nigericin (15 µM) and K^+ (135 mM). (B) Changes in ΔF/F in dependence of pH_i. Exemplary averaged calibration curve of 16 single cells (n_{exp} = 6).

3.1.2 pH_i regulation is Na^+-dependent

To identify mechanisms of pH_i regulation in sperm, I first used the NH_4-prepulse/acid load method (Boron, 2004; Boron and De Weer, 1976). Figure 6 shows a single pHrodo-Red-loaded sperm which was first kept in physiological ES (pH 7.35) and a stable pH_i was recorded. Exposure to 15 mM NH_4Cl rapidly alkalized the cell, visible as a reduction of ΔF/F (Figure 6). Because the conjugate base/acid pair NH_3/NH_4^+ has a pK_a = 9.4, only a very small percentage of NH_4^+ dissociates to $NH_3 + H^+$ at pH = 7.35. Nevertheless, the neutral NH_3, but not NH_4^+, rapidly diffuses across the membrane. In the cytosol, NH_3 serves as an H^+ acceptor, and a new equilibrium $NH_3 + H^+ \leftrightarrow NH_4^+$ is established, thereby alkalizing the cell. During exposure to NH_4Cl, a slow re-acidification process was observed in many but not all sperm. A slow uptake of NH_4^+ (Boron & De Weer, 1976) or an alkalization-induced, compensatory downregulation of Na^+/H^+ exchange activity (Aronson et al., 1982) might contribute to re-acidification during NH_4Cl exposure. After washing out NH_4Cl by reperfusion with ES, sperm acidified due to the fast diffusion of NH_3 out of the cell, "trapping" of intracellular NH_4^+, and thereby accumulating H^+ intracellularly. Subsequently, the pH_i slowly returned to resting pH_i within 1,170 ± 290 s (Figure 6A; n_{exp} = 3, n_{cells} = 8). Interestingly, the re-acidification during NH_4Cl exposure was less obvious or absent in cells that showed a smaller or no acidic overshoot after wash-out of NH_4Cl. I restricted analysis to cells

with a strong acidic overshoot. pH_i recovery from acid load was prevented by either replacing Na^+ with NMDG, or by amiloride, a blocker of Na^+/H^+ exchangers like NHE1 (Frelin et al., 1988; Pedersen and Counillon, 2019). When the solution was changed back to physiological ES, pH_i recovered from the acid load (Figure 6B). These experiments suggest that an amiloride-sensitive Na^+/H^+ exchange is involved in the pH_i regulation of human sperm.

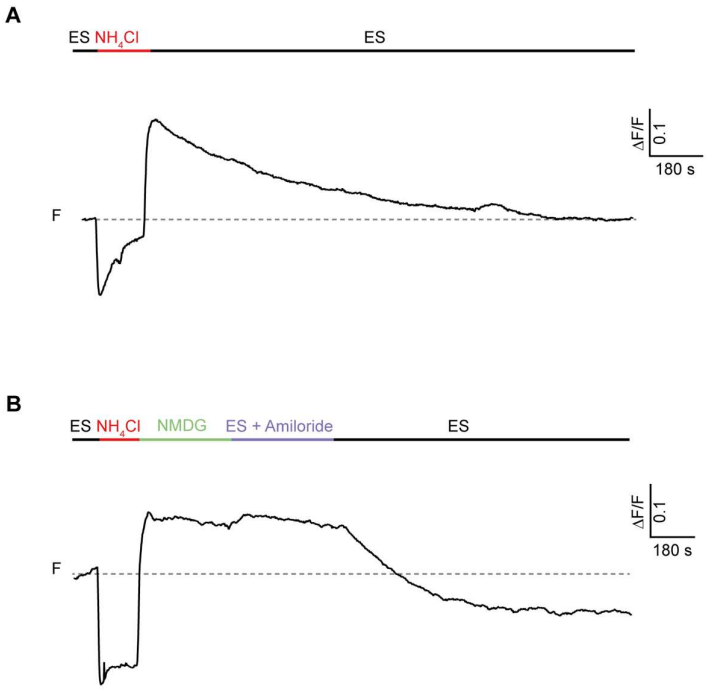

Figure 6. Re-alkalization after an acid-load is driven by Na^+/H^+ exchange. (A) Changes in ΔF/F after superfusion of a sperm cell with ES containing NH_4Cl (15 mM); the cell first alkalizes, then acidifies ("acid-load") after removal of NH_4Cl from the bath, and eventually returns to basal pH_i levels. (B) NMDG and amiloride, a Na^+/H^+ exchange blocker, prevent recovery from the acid load. Sequential perfusion with ES, ES/NH_4Cl, NMDG-ES, ES + amiloride, and ES.

Given a high extracellular and a low intracellular Na^+ concentration, Na^+/H^+ exchange is a candidate mechanism to facilitate capacitation-associated alkalization by exchanging ions along their gradients (Aronson et al., 1982). From vagina to oviduct, pH_o increases by more than one unit (reviewed by Ng et al., 2018). To mimic this pH_o change and to study its influence on sperm, I exposed cells to a pH_o range from 6.5 to 7.7 (Figure 7A). In response to pH_o = 7.7, pH_i slowly increased from $pH_i = 6.8 \pm 0.1$ to $pH_i = 7.1 \pm 0.2$ ($n_{exp} = 7$; $n_{cells} = 16$, and $n_{exp} = 6$; $n_{cells} = 21$, respectively) with a half-time $t_{1/2} = 830 \pm 510$ s ($n_{exp} = 3$, $n_{cells} = 20$; Figure 7A-C). Similar to the NH_3/NH_4^+-acid load experiment, amiloride prevented pH_i adjustment, confirming the idea that human sperm regulate pH_i by an amiloride-sensitive

Na^+/H^+ exchanger (Figure 7A, second trace). Sperm loaded with the fluorescent Na^+-indicator Asante NaTRIUM Green-2 (ANG2)-AM exposed to the same pH_o change displayed a $[Na^+]_i$ increase roughly following the kinetics of alkalization ($t_{1/2}$ = 600 ± 320 s, n_{exp} = 5; n_{cells} = 25; Figure 7A, green trace, B), again suggesting the involvement of a Na^+/H^+ exchanger.

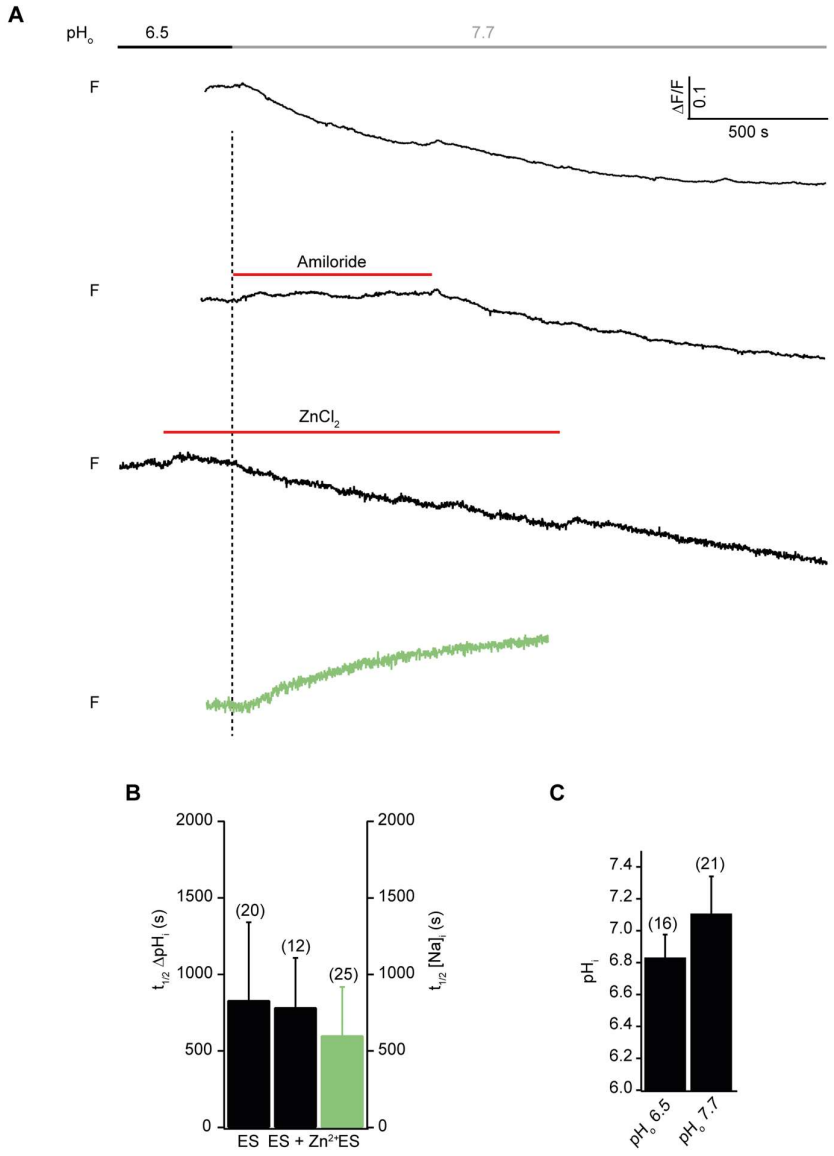

Figure 7. pH_i follows pH_o increase via Na^+/H^+ exchange. (A) Changes in pH_i (black traces) and $[Na^+]_i$ (4th trace, green) upon a switch from pH_o 6.5 to pH_o 7.7. Amiloride (500 µM) completely prevented alkalization (2nd trace) and Zn^{2+} (100 µM) had no effect (3rd trace). (B) Half-time $t_{½}$ (mean ± s.d.) of ΔpH_i (left ordinate) and $\Delta[Na^+]_i$ (right ordinate for right bar, green) upon change from pH_o 6.5 to pH_o 7.7; Zn^{2+} (100 µM; number of cells indicated in parentheses; n_{exp} = 3, 4, and 5, respectively). (C) Final pH_i (mean ± s.d.) after incubating sperm for 30 min at the indicated pH_o in absence of inhibitors.

It was suggested that Hv1 alkalizes sperm during capacitation, leading to the increased pH_i that is necessary for CatSper opening (Lishko et al., 2010). Inhibition of Hv1 with zinc (Ramsey et al., 2006) during the exposure to pH 7.7 did not prevent alkalization (Figure 7A, third trace, B): The time course of alkalization in zinc is similar to the time course of alkalization in the absence of zinc (780 ± 320 s, n_{exp} = 4, n_{cells} = 12), indicating no involvement of Hv1 during the slow intracellular alkalization following exposure to a higher pH_o. The tested conditions however, as well as the conditions in the female reproductive tract, emulated in the experiment, do not promote Hv1 opening by depolarization, but leave the possibility of a pH gradient large enough to shift the Hv1 open probability to a more negative V_m (Berger et al., 2017).

3.1.3 Voltage-dependent pH_i regulation

In contrast to voltage-gated channels, ion exchangers transport ions by a simple alternate-access mechanism that is not gated by voltage. However, the ion exchange may be electrogenic, i.e., no electroneutral exchange, and thus, by definition, voltage-dependent. Surprisingly, like Hv1 or other voltage-gated channels, sNHE contains a VSD and might serve as voltage-gated pH regulator in human sperm (Lishko et al., 2010; Wang et al., 2003). To test whether these two proteins regulate pH_i in a voltage-dependent fashion, I combined fluorometric pH recording with the patch-clamp technique (patch-clamp fluorometry, PCF, Figure 8A). Patch-clamping allows recording currents across the membrane and has been used to identify proton and other ion conductances in human sperm (Berger et al., 2017; Brenker et al., 2012; Kirichok et al., 2006; Lishko et al., 2010). In addition, loading sperm with pHrodo-Red via the patch pipette allows the simultaneous detection of relative changes in pH_i by recording changes in fluorescence intensity. Because pHrodo-Red was not available as a salt, I used the thiol-reactive form pHrodo-Red maleimide, which can bind to proteins' thiol groups. Binding to proteins inside the cell might help to establish a stable pHrodo-Red concentration by minimizing diffusion of pHrodo-Red back into the pipette. After establishing the whole-cell mode, the fluorescence intensity rose mono-exponentially in the head and flagellum and levelled off after several minutes ($t_{1/2head}$ = 69 ± 42 s, $t_{1/2flag}$ = 106 ± 52 s, n_{cells} = 5; Figure 8B), indicating that pHrodo-Red accumulated inside the cell and reached a stable concentration level.

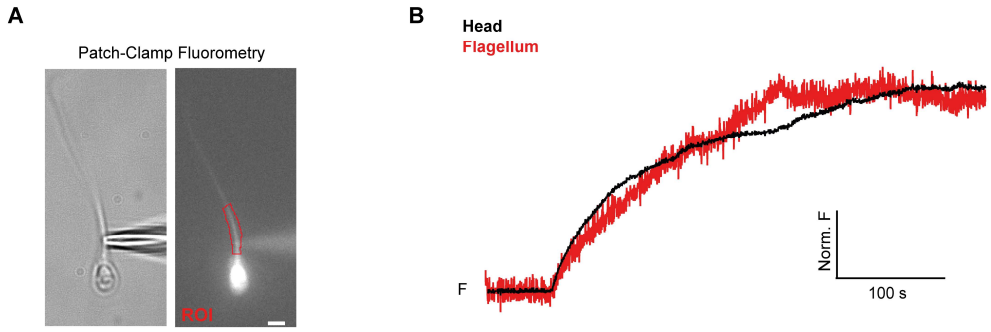

Figure 8. Establishing patch-clamp pH fluometry in human sperm. (A) Patch-clamp fluorometry. Bright-field microscopy (left) and fluorescence image (right) of a human sperm cell loaded with pHrodo-Red (12.5 µM); scale bar 3 µm. (B) Time course of fluorescent change during solution exchange between pipet and sperm head (black) and flagellum (red) by patch-clamp fluorometry after break-in. The pipet was filled with 12.5 µM of pHrodo-Red-maleimide and the holding potential V_m was -30 mV.

In all PCF recordings, the fluorescence intensity was highest in the head. In addition, fluorescence intensity slightly declined towards the tail, possibly due to a gradually declining diameter of the flagellum and, therefore, a declining amount of dye. Additionally, only the head of the cell is fixed on the coverslip, so that the thin flagellum is able to move out of the focal plane, which could also contribute to a lower fluorescence intensity (Figure 8A). The intracellular solution (IS) was composed to support opening of Hv1 during depolarization as well as a potential hyperpolarization-activated Na^+/H^+ exchange. Since Hv1 channels open exclusively at V_m values positive to the Nernst potential for protons (Berger et al., 2017), pH_i of 6.5 provided an outward-directed 8-fold proton gradient and thereby a sufficient proton gradient for Hv1 opening during depolarization and a driving force for H^+ efflux. $[Na^+]_i$ = 1.4 mM established an inward-directed 100-fold Na^+ gradient. In case of a voltage-gated Na^+/H^+ exchange, Na^+ and H^+ gradients would both support and influx of Na^+ and simultaneous efflux of H^+, leading to an intracellular alkalization. During the break-in and dye-loading process, cells were held at V_{hold} = -30 mV, which is close to the physiological resting membrane potential (~-40 mV; Linares-Hernández et al., 1998) and should neither activate Hv1 (Lishko et al., 2010) nor sNHE (Windler et al., 2018).

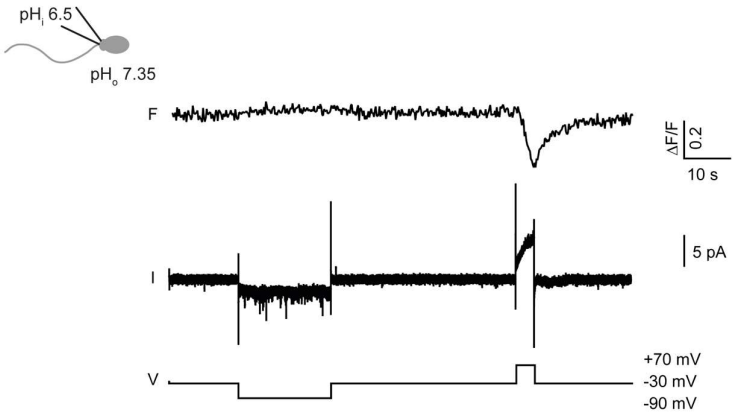

Figure 9. Voltage-dependent pH_i control: depolarization activates an Hv1-induced alkalization but hyperpolarization had no effect on the pH_i. Changes in pHrodo-Red fluorescence (F) and current (I) during a hyper- (-90 mV) and depolarizing (+70 mV) voltage step from V_{hold} = -30 mV. pH_o = 7.35; pH_i = 6.5.

First, cells were hyperpolarized for 20 s to -90 mV to open the putatively hyperpolarization-activated sNHE. In sea urchin, the Na^+/H^+ exchange is electroneutral in either direction. Given the chosen ionic gradients, I expected that activation of sNHE by hyperpolarization would alkalize the cell. However, none of the recorded cells (n_{cells} = 10) alkalized during the 20 s long stimulus, suggesting that no voltage-dependent Na^+/H^+ exchange is present in human sperm. A depolarizing voltage step to +70 mV, however, robustly elicited an outward current and a fluorescence decrease, i.e., simultaneous alkalization, which rapidly recovered during repolarization (Figure 9). Outward current and alkalization were inhibited by 100 µM zinc, suggesting that this current is carried by Hv1 (Figure 10).

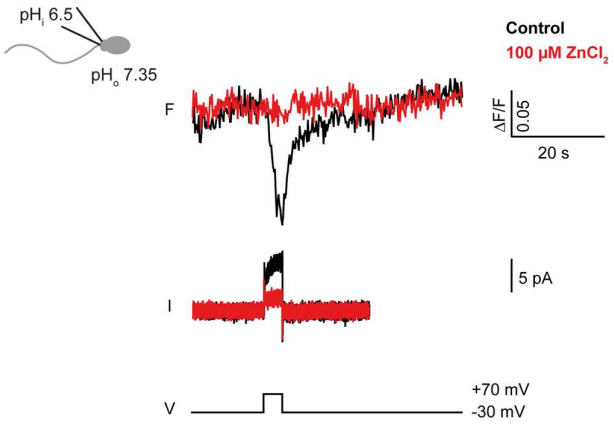

Figure 10. Hv1 blocker zinc inhibits Hv1 current and depolarization-induced alkalization in human sperm. Changes in pHrodo-Red fluorescence (F) and current (I) during depolarization to +70 mV to activate Hv1 in the absence (black) and presence of Zn^{2+} (100 µM; red). pH_o = 7.35; pH_i = 6.5.

Hv1 is only expressed in the principal piece (Lishko et al., 2010); nevertheless, the Hv1-mediated fluorescence signal not only spread along the flagellum but was also clearly detectable in the head (Figure 11A-C), suggesting that Hv1-mediated alkalization and proton diffusion is not restricted to the principal piece. The half-time $t_{1/2}$ of the Hv1-mediated alkalization increases with distance to the pipette (Figure 11D). The flagellum area around the patch pipette (principal piece, green) showed the largest and fastest fluorescence signal and was chosen for analysis of PCF experiments (Figure 11B-D).

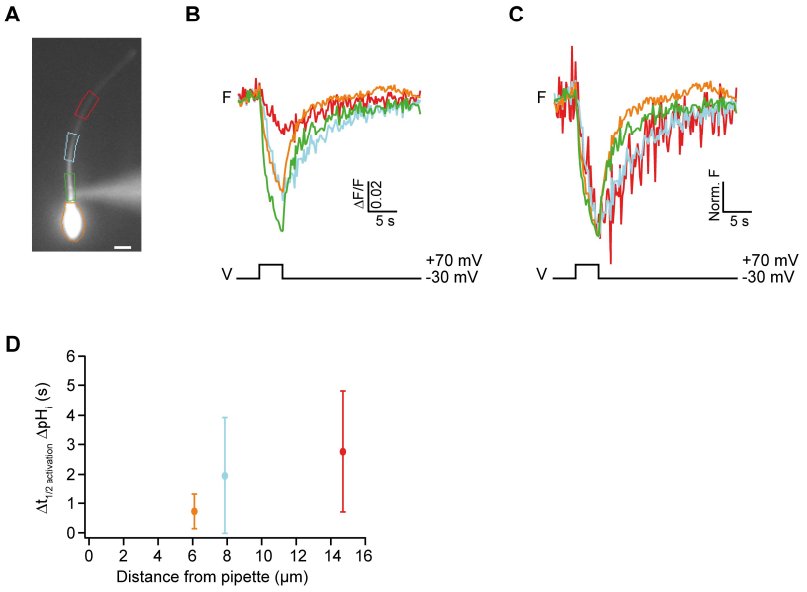

Figure 11. Hv1-induced alkalization spreads along sperm flagellum. (A) pHrodo-Red-loaded human sperm with attached patch pipette and manually chosen ROIs. (B) Alkalization induced by a +70 mV depolarization step and subsequent Hv1 activation during PCF recording in presence of CO_2/HCO_3^- (5%/25 mM); pH_o = 7.35; pH_i = 6.5. Superposition of fluorescent signal of different ROIs. (C) Normalized superposition of fluorescent signals from B. (D) Difference of $t_{1/2}$ (mean ± s.d.) of Hv1 induced alkalization activation from respective ROIs compared to ROI at the pipette (green, n_{cells} = 3).

3.2 Hv1 and the $CO_2 + H_2O \leftrightarrow HCO_3^- + H^+$ equilibrium

3.2.1 CO_2/HCO_3^- wash-in acidifies rather than alkalizes sperm

A major physiological pH buffer is bicarbonate (HCO_3^-); its concentration is coupled to the CO_2 partial pressure (pCO_2) by the equilibrium $CO_2 + H_2O \leftrightarrow HCO_3^- + H^+$. Inside and outside of many cells including sperm, the reaction is catalyzed in both directions by the CA. In sperm, HCO_3^- activates sAC, which increases cAMP (Chen et al., 2000), providing an intriguing link between pH_i and intracellular signaling. In most tissues, pCO_2 is relatively constant at around 40 mmHg under physiological conditions (Boron, 2016). Assuming the solubility coefficient of CO_2 in water is 0.05, according to Henry's

law, a pCO_2 of 40 mmHg is equivalent to a CO_2 concentration of 1.2 mM (Boron, 2016). With the simplifying assumption that CO_2/HCO_3^- is the only pH buffer, the pH is solely determined by the CO_2 and the HCO_3^- concentrations according to the Henderson-Hasselbach equation (Equation 2) with $pK_a = 6.1$. Thus, at a given pH and a given pCO_2, the HCO_3^- concentration is predetermined. To better mimic the pH and HCO_3^- change during the journey through the female reproductive tract, I repeated the pH_o exchange experiment, shown in Figure 7, in the presence of a constant physiological pCO_2 by continuously gassing the extracellular solutions with 5% CO_2/95% O_2 ("carbogen") and the respective HCO_3^- concentration, according to Henderson-Hasselbalch (Equation 2; pH 6.5 + 3 mM HCO_3^-; pH 7.7 + 30 mM HCO_3^-). In the whole organism, CO_2/HCO_3^- in principle is an open buffer system because excessive CO_2 can be rapidly exhaled via the lungs. As a consequence, at the cellular level, pCO_2 remains relatively constant, and I refer to this condition as a quasi-closed system (Figure 12).

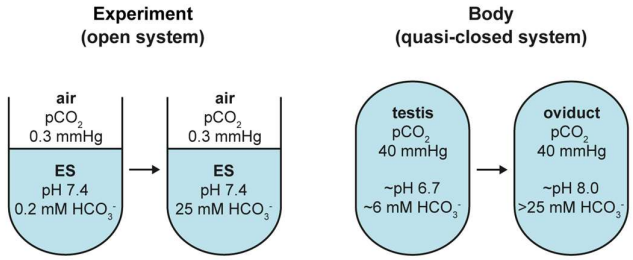

Figure 12. CO_2, HCO_3^- and pH are interconnected in a (quasi)-closed system. Scheme of the difference between an open experimental system in equilibrium with air (pCO_2 = 0.3 mmHg) and a quasi-closed system in equilibrium with body fluid (pCO_2 = 40 mm Hg).

I exposed pHrodo-Red AM-loaded sperm first to an epididymis-like solution ES/pH_o 6.5 (5% CO_2 + 3 mM HCO_3^-), then switched to an oviduct-like medium ES/pH_o 7.5 (5% CO_2 + 30 mM HCO_3^-) and thus roughly emulated the physiological transition between epididymis and oviduct with respect to pH and HCO_3^-. The pH_i slowly increased from 6.6 ± 0.1 to 7.0 ± 0.1 (Figure 13A (blue trace), B). The average magnitude and time course of ΔpH_i and the final pH_i in the presence or absence of CO_2/HCO_3^- were similar (ΔpH = 0.3 and 0.4; $t_{1/2}$ = 830 ± 510 and 680 ± 642 s, and final pH_i = 7.1 and 7.0, respectively; Figure 13B & C). Thus, the presence of HCO_3^- and CO_2 does not significantly alter the slow intracellular adjustment to alkaline pH_o driven by Na^+/H^+ exchange.

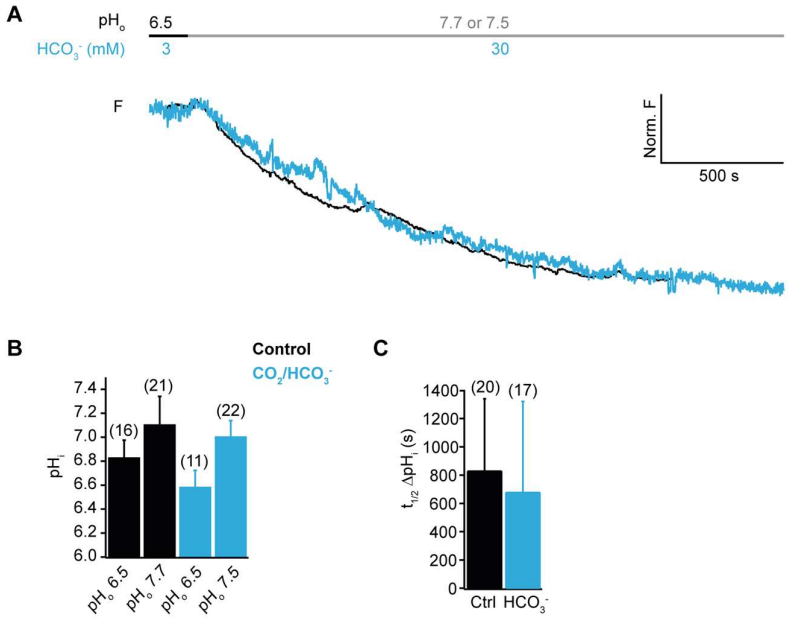

Figure 13. Diffusion of CO_2 across membrane controls pH_i homeostasis. (A) Time course of alkalization after a switch from pH_o 6.5 to pH_o 7.7 (control, black) and in the presence of CO_2/HCO_3^- (5%/25 mM; blue). (B) Final pH_i (mean ± s.d.) after incubating sperm for 30 min at the indicated pH_o in the absence (black) or presence of CO_2/HCO_3^- (pH_o 6.5 + 5%/3 mM or pH_o 7.5 + 5%/30 mM; blue). Number of cells indicated in parentheses. (C) Half-time $t_{1/2}$ of ΔpH_i (mean ± s.d.) upon a switch from pH_o 6.5 to pH_o 7.7 without (black) and from pH_o 6.5 to pH_o 7.5 with HCO_3^-/CO_2 (3 mM/5% and 30 mM/5%, blue). Number of cells indicated in parentheses.

The mouse sNHE has been proposed to be functionally and structurally connected with the HCO_3^--activated sAC (Chen et al., 2000; Wang et al., 2007). Moreover, mammalian sNHEs carry a CNBD at the intracellular C-terminus, suggesting that the Na^+/H^+ exchange is regulated by cyclic nucleotides. Thus, sNHE activity could be regulated by HCO_3^- (or vice versa). Indeed, in sea urchin sperm, the activation of sNHE is shifted towards more depolarized potentials by cyclic-nucleotide binding (Windler et al., 2018). To this end, I investigated a putative activation of sNHE by cyclic nucleotides via sAC in human sperm. I exposed patch-clamped sperm to ES containing 25 mM HCO_3^- (HCO_3^--ES; 5% CO_2) and applied a hyperpolarizing voltage step to -90 mV. This condition reflects the high HCO_3^- concentration in the uterus and oviduct and HCO_3^- should stimulate cAMP production via sAC. By continuously bubbling the solution with 5% CO_2, I mimicked the pCO_2 in the body and simultaneously kept the pH and the HCO_3^- concentration constant (pH 7.35 + 25 mM HCO_3^-). However, hyperpolarization in presence of HCO_3^- did not result in a detectable change in pH_i and did not induce any current (Figure 14A, blue trace).

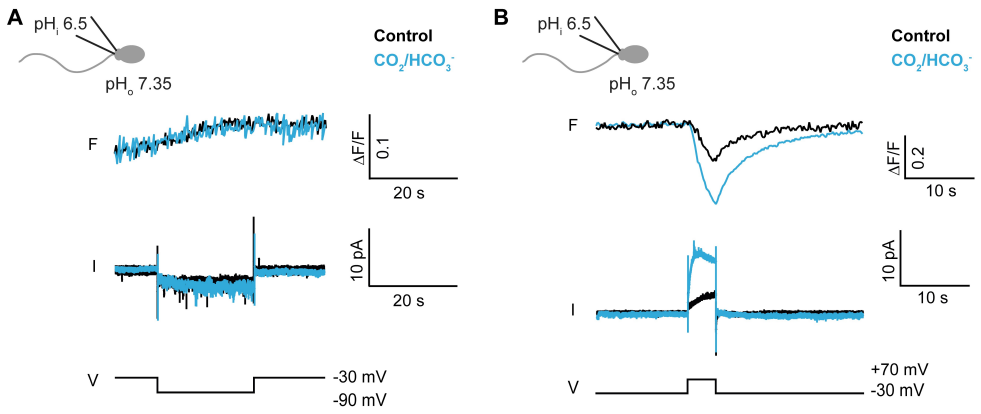

Figure 14. CO_2/HCO_3^- does not stimulate hyperpolarization-induced Na^+/H^+ exchange but enhances proton currents in human sperm. (A) PFC recording of human sperm during exposure to CO_2/HCO_3^-. Changes in fluorescence of pHrodo-Red and current after stepping voltage from V_m = -30 mV to -90 mV to activate sNHE in the absence (black) and presence of CO_2/HCO_3^- (5%/25 mM; blue). pH_o = 7.35; pH_i = 6.5. (B) PFC recording of human sperm during exposure to CO_2/HCO_3^-. Changes in fluorescence of pHrodo-Red and current after stepping voltage from Vm = -30 mV to +70 mV to activate sNHE in the absence (black) and presence of CO_2/HCO_3^- (5%/25 mM; blue). pH_o = 7.35; pH_i = 6.5.

In contrast, CO_2/HCO_3^- wash-in increased the depolarization-induced Hv1 outward current and concomitant alkalization (Figure 14B). There are two possible explanations for this observation: 1) CO_2/HCO_3^- wash-in acidifies the cell and therefore the driving force for the proton current was increased, or 2) HCO_3^- directly or indirectly modulates the opening probability of Hv1, e.g. via phosphorylation by PKA. A modulation of the opening probability of Hv1 seems unlikely because no PKA phosphorylation sites in the Hv1 protein are known. A phosphorylation site for PKC has been reported (Musset et al., 2010), but PKC is not activated by HCO_3^- and not present in human sperm. In contrast, wash-in of CO_2/HCO_3^- can lead to acidification if CO_2 enters the cell faster than HCO_3^-. Fast CO_2 diffusion across the membrane is plausible; HCO_3^- influx requires, due to its charge, a channel or a carrier protein. Previous studies suggested HCO_3^- entry via an anion exchanger or CFTR (Demarco et al., 2003; Li et al., 2010; Puga Molina et al., 2018b, 2017). However, the increase of Hv1 proton current suggests that acidification by CO_2 diffusion is the dominant mechanism rather than alkalization by HCO_3^- transport. After repolarization, pH_i returned to baseline levels in presence and absence of CO_2/HCO_3^- (Figure 14B). Of note, the tail current of Hv1 is almost absent and, therefore, cannot account for the reacidification. Thus, a different mechanism is underlying the recovery.

In order to confirm intracellular acidification caused by CO_2/HCO_3^-, I monitored pH_i while changing the bath solution from ES to ES-HCO_3^- (5% CO_2/25 mM HCO_3^-). Figure 15A shows that indeed, sperm rapidly acidified when exposed to ES-HCO_3^- and

stayed at a lower pH_i as long as the exposure lasted, suggesting that CO_2 diffusion into the cell and subsequent readjustment of the HCO_3^-/CO_2 equilibrium and acidification is the major source of HCO_3^- intracellularly. Even when recording for 30 min, the cells maintained a lower pH_i (Figure 15B). The ΔpH_i was -0.11 ± 0.06 (n_{exp} = 10; n_{cells} = 49) with a time constant τ_{sperm} = 5.6 ± 2.2 s (n_{exp} = 10; n_{cells} = 42, Figure 16A, B).

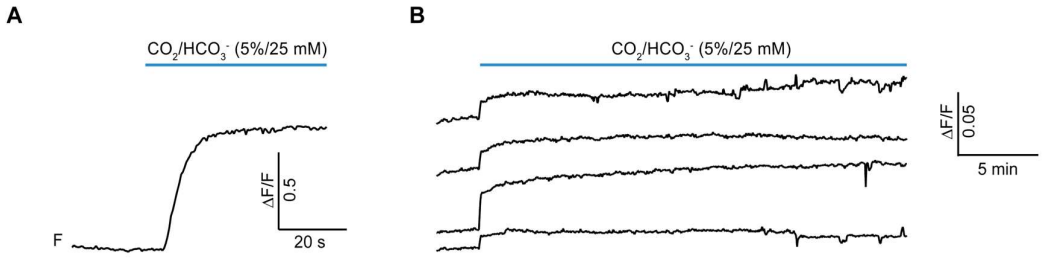

Figure 15. CO_2/HCO_3^- acidifies sperm via CO_2 diffusion and CA activity. (A) Changes in fluorescence of a pHrodo Red-labeled human sperm upon switching the bath from pH_o 7.35 to pH_o 7.35/CO_2/HCO_3^- (5%/25 mM). (B) Changes in fluorescence of pHrodo Red-labeled human sperm upon long-term exposure to pH_o 7.35 to pH_o 7.35/CO_2/HCO_3^- (5%/25 mM).

Inhibiting Hv1 (by Zn^{2+}), CFTR (by $CFTR_{inh}$-172), HCO_3^- transporters (by DIDS), or Na^+/H^+ exchangers (by amiloride), did not significantly change the amplitude or the time constant of the HCO_3^--induced pH_i change (Figure 16A, B). If any, the change was slightly larger and faster with zinc, which might be due to the fact that zinc acts as a cofactor for several isoforms of the CA and might thereby accelerate CA activity (Christianson and Fierke, 1996).

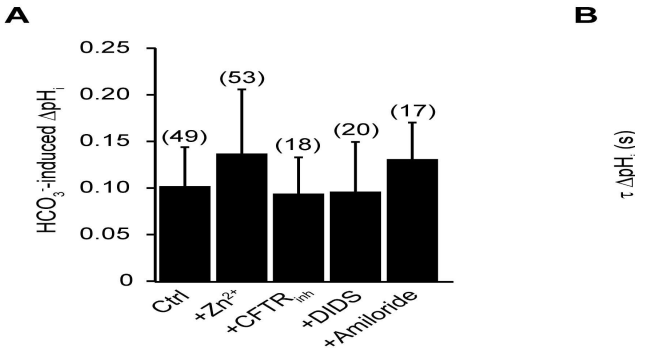

Figure 16. Inhibition of Hv1, CFTR, HCO_3^-/Cl^- or Na^+/H^+ exchangers does not alter the CO_2/HCO_3^--induced acidification. (A) HCO_3^- -induced ΔpH_i (mean ± s.d.) upon switching from pH_o 7.35 to pH_o 7.35/CO_2/HCO_3^- (5%/25 mM) in the presence of various inhibitors. Hv1 inhibitor Zn^{2+} (100 µM), CFTR inhibitor $CFTR_{inh}$-172 (100 µM), SLC4 inhibitor DIDS (100 µM), and SLC9A/B inhibitor amiloride (500 µM; number of cells indicated in parentheses; n_{exp} = 10, 11, 3, 4, and 4, respectively). (B) Time constant τ of ΔpH_i of panel (A).

Similar experiments using HEK and CHO cells also resulted in robust acidification by CO_2/HCO_3^- and the pH_i of all tested cell types increased again after changing back to physiological ES, suggesting a general mechanism that is not sperm-specific

(Figure 17A, B). The time course of acidification in sperm was close to the mixing time of the bath solution (measured by washing-in the fluorescent dye Alexa488, Figure 17A, B, green trace), suggesting that the perfusion, not the diffusion of CO_2 over the membrane, limits the kinetics of the pH change. The time course of acidification in HEK was 2.2-fold slower than in sperm (Figure 17C; τ_{HEK} = 12.3 ± 1.6 s, n_{exp} = 4, n_{cells} = 38). Remarkably, the time course of acidification in CHO cells was even 9.4-fold slower than in sperm and 4.2-fold slower than in HEK cells (τ_{CHO} = 52 ± 20 s, n_{exp} = 5, n_{cells} = 64). Because size and geometry of HEK and CHO cell are rather similar compared to sperm, the large difference in the time course of acidification between HEK and CHO cells cannot be accounted for by the difference in membrane-surface ratio which might affect acidification speed. Inhibition of HCO_3^- transporters did not change the acidification amplitude or time course in sperm, suggesting that diffusion of CO_2 into the cell is responsible for the acidification (Figure 16). CAII and CAIV are functionally expressed in sperm (Wandernoth et al., 2015, 2010) and should catalyze the fast acidification during exposure to CO_2/HCO_3^-. To test an involvement of CA in CO_2/HCO_3^--induced acidification, I exposed sperm, HEK, and CHO cells to CO_2/HCO_3^- in presence of the CA inhibitor acetazolamide (ACZ) and compared the time course of acidification. In sperm and in HEK cells, ACZ slowed down the acidification kinetics by 7.0- and 5.5-fold, respectively. In CHO cells, ACZ slowed the acidification kinetics by only 1.1-fold (Figure 17C). The acidification time constants in sperm and HEK cells in the presence of ACZ were approximately in the range of the acidification time constant of CHO cells in absence or presence of ACZ. These data suggest that upon CO_2/HCO_3^- perfusion, CO_2 rather than HCO_3^- enters the sperm cell. CO_2 hydration is catalyzed by CA activity, and the resulting H_2CO_3 rapidly dissociates into HCO_3^- and H^+, which acidifies the cytosol. The slow CO_2/HCO_3^- -induced acidification of CHO cells suggests a low expression of CA in CHO cells but needs further experimental confirmation.

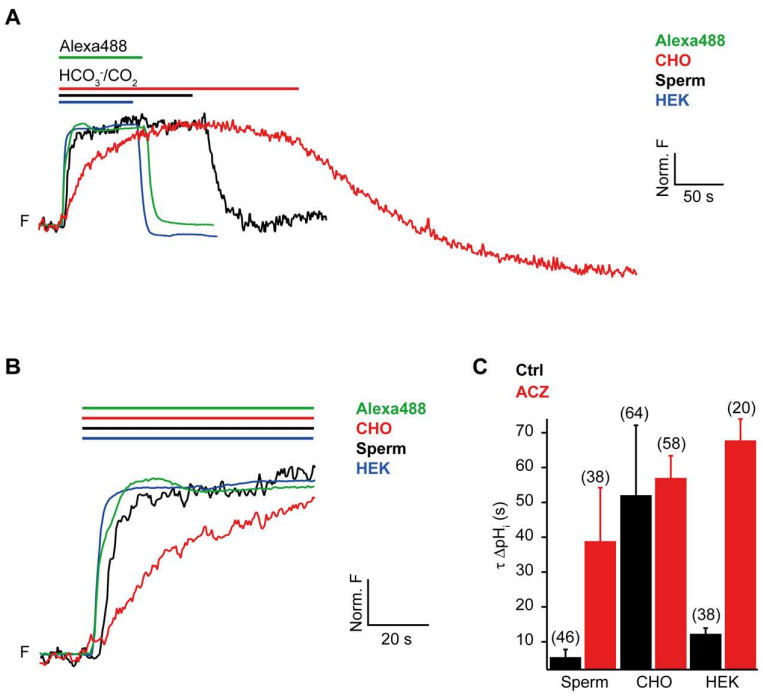

Figure 17. HCO_3^-/CO_2 acidifies HEK and CHO cells. (A) Normalized changes in pHrodo-Red fluorescence upon switching the bath from pH_o 7.35 to pH_o 7.35/CO_2/HCO_3^- (5%/25 mM) in sperm (black), HEK293 cells (blue), and CHO cells (red). The green trace shows the mixing kinetics in the recording chamber while washing-in the fluorescent dye Alexa488. (B) Extended time scale of panel (A). (C) Time constants τ (mean ± s.d.) of ΔpH_i upon switching from pH_o 7.35 to pH_o 7.35/CO_2/HCO_3^- solution in the absence (black) or presence of ACZ (100 µM, red) in human sperm, CHO, and HEK293 cells (number of cells indicated in parentheses; n_{exp} = 10, 9, 5, 3, 4, and 2, in presented order).

Next, I used the PCF method to study voltage- and CO_2/HCO_3^--dependent pH regulation in mouse sperm. Mouse sperm lack Hv1-mediated proton currents (Lishko et al., 2010) but express the sNHE SLC9C1 (Wang et al., 2003). I recorded from wildtype (wt) and SLC9C1$^{-/-}$ mouse sperm (Wang et al., 2003). Surprisingly, both wt and SLC9C1$^{-/-}$ sperm displayed similar behavior. Superfusion with CO_2/HCO_3^- evoked rapid acidification, whereas de- or hyperpolarizing voltage steps did not evoke currents or pH_i changes, neither before nor after CO_2/HCO_3^- treatment (Figure 18). These experiments confirmed the absence of Hv1 currents in mouse sperm (Lishko et al., 2010), and furthermore showed that sNHE, similar to human sperm, does not serve as voltage-gated Na^+/H^+ exchanger in mouse sperm.

In conclusion, at physiological pCO_2, rapid CO_2 diffusion across sperm membrane and high CA activity controls pH_i, whereas HCO_3^--influx via anion exchangers or CFTR channels could not be detected experimentally. Neither in human, nor mouse sperm, a voltage-dependent Na^+/H^+ exchange was recorded.

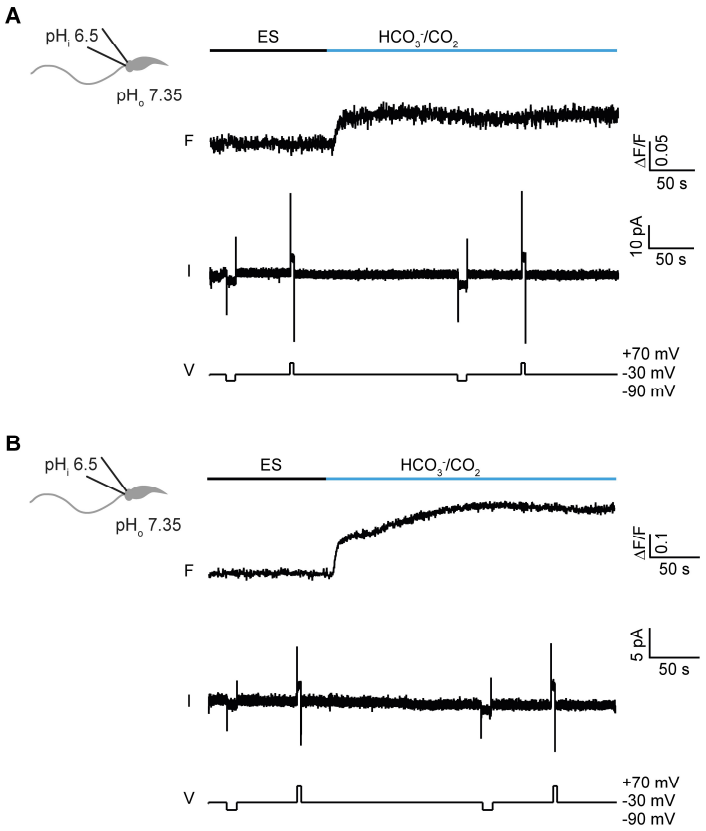

Figure 18. Na^+/H^+ exchange via sNHE in mouse sperm is not voltage-gated. (A) PCF recording from sperm of a wt mouse during superfusion with ES (black bar) and CO_2/HCO_3^- (5%/25 mM; blue bar). Changes in pH_i (upper) and currents (lower). The V_m was first stepped from a holding potential of -30 mV to -90 mV to activate putative voltage-gated SLC9C1, followed by a step from -30 mV to +70 mV to activate Hv1. pH_o = 7.35; pH_i = 6.5. (B) Similar recordings as panel A from sperm of a SLC9C1$^{-/-}$ mouse.

3.2.2 CO_2/HCO_3^--induced acidification enhances Hv1 activity

The function of Hv1 is still enigmatic (Florman et al., 2010) and it is unlikely that Hv1 contributes to the alkalization that has been suggested to take place during the capacitation process. However, due to the unique mechanisms that control the open probability of Hv1 (P_o), an acidification rather than depolarization might activate Hv1. I further investigated the connection between Hv1 activity and the $CO_2/HCO_3^-/H^+$ equilibrium. P_o of Hv1 depends on both V_m, and the pH difference ($\Delta pH = pH_o - pH_i$) across the cell membrane (Cherny et al., 1995; Ramsey et al., 2006). At $\Delta pH = 0$, Hv1 opens at ca. +30 mV (V_{thr} = +30 mV). A positive ΔpH shifts the activation curve to more negative potentials; a negative ΔpH shifts the activation curve to more positive potentials. ΔpH therefore co-determines P_o and the electromotive force ε. Setting a positive ΔpH by exposing sperm to CO_2/HCO_3^--induced acidification should enhance Hv1 activity.

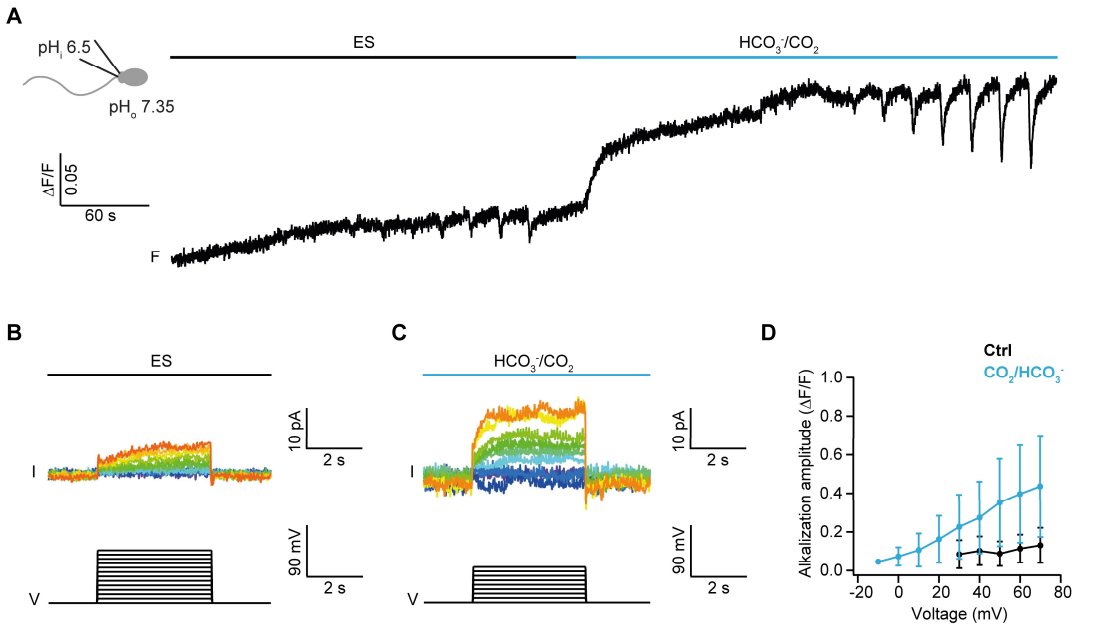

Figure 19. Hv1 activity is transiently enhanced by CO_2/HCO_3^-. (A-C) PCF recording of human sperm. Voltage-dependence of pH_i responses (A) and Hv1 currents (B&C) before (B) and during (C) superfusion with CO_2/HCO_3^- (5%/25 mM) solution. V_m was stepped for 4 s from -30 mV to +70 mV in increments of 10 mV. pH_o = 7.35; pH_i = 6.5. (D) Normalized amplitude ΔF/F (mean ± s.d.) of voltage-evoked changes in ΔpH_i under ES (control, black) and CO_2/HCO_3^- (blue) conditions (n_{cells} = 7).

I determined the voltage-dependence in absence and presence of CO_2/HCO_3^- by applying voltage steps with +10 mV increments, starting at -30 mV (Figure 19A-C). In absence of CO_2/HCO_3^-, alkalization was first detectable at +30 mV, whereas in presence of CO_2/HCO_3^-, alkalization was already detectable at -10 mV. Hv1 currents and pH_i signals increased up to 10-fold in the presence of CO_2/HCO_3^- (Figure 19D). This suggests, that CO_2/HCO_3^- enhances proton currents by increasing P_o and ε. A prolonged depolarization, however, did not lead to stronger alkalization even when the outward current stayed constant, suggesting that the Hv1-mediated proton outward current is balanced by an electroneutral process that re-acidifies the cytosol such that a new pH equilibrium is reached (Figure 20). After repolarization, pH_i quickly returned to starting pH_i values but no Hv1 tail current could be recorded. This undermines the existence of an electroneutral process regulating pH_i.

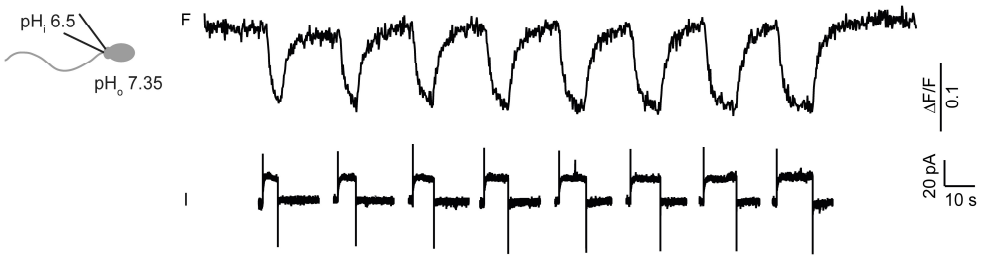

Figure 20. Hv1-induced alkalization saturates during constant depolarization and quickly recovers after repolarization. PCF recording of pHrodo-Red loaded human sperm in presence of CO_2/HCO_3^- (5%/25 mM) during multiple +70 mV depolarization steps with increasing length. pH_o = 7.35; pH_i = 6.5.

To narrow down which components play a role in the pH_i regulation during Hv1 activity, I first compared the alkalization and acidification kinetics during a voltage stimulus. Interestingly, the alkalization and acidification kinetics (Figure 21A, grey trace) were slower than the currents (Figure 21A black trace; $t_{1/2al}$ = 2.5 ± 1.0 s, n_{cells} = 13; $t_{1/2ac}$ = 2.5 ± 1.2 s, n_{cells} = 7). Next, I used amiloride to inhibit Na^+/H^+ exchange during de- and repolarization. However, the half-times were not altered by the blocker ($t_{1/2al}$ = 2.6 ± 0.1 s, n_{cells} = 2; $t_{1/2ac}$ = 2.6 ± 0.1 s, n_{cells} = 2, not shown).

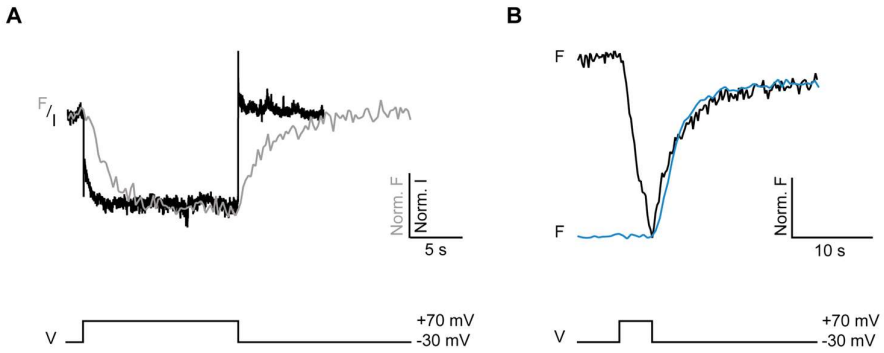

Figure 21. The $CO_2/HCO_3^-/H^+$-equilibrium strongly buffers pH_i in human sperm. (A) Superposition of the time course of changes in pH_i (grey) and Hv1 currents (black) after stepping V_m from -30 mV to +70 mV for 15 s. Current trace was flipped horizontally. pH_o = 7.35; pH_i = 6.5. (B) Superposition of the time course of normalized acidification during exposure of sperm to CO_2/HCO_3^- (5%/25 mM; blue) or termination of the V_m pulse (black) during a PCF experiment (pH_o = 7.35; pH_i = 6.5.). Traces origin from different cells.

Intriguingly, the kinetics of depolarization-induced reacidification (Figure 21B, black trace) and the kinetics of CO_2/HCO_3^--induced acidification were largely similar (blue trace). The time course of CO_2/HCO_3^--induced acidification is largely determined by the CA (Figure 17C). To test, whether CO_2 diffusion across the membrane and intracellular conversion by CA contributes to the reacidification after repolarization, I used ACZ to inhibit the CA during depolarization (Figure 22). ACZ slowed down the pH change, the reacidification stronger than the alkalization, and decreased the outward proton

current ($t_{1/2al}$ = 3.6 ± 1.3 s, $t_{1/2ac}$ = 5.4 ± 2 s, n_{cells} = 4; Figure 22A, B). The reacidification was slowed down 2.1-fold by ACZ. In contrast, the HCO_3^-/CO_2^--induced acidification was slowed down 7.0-fold by ACZ (Figure 17C).

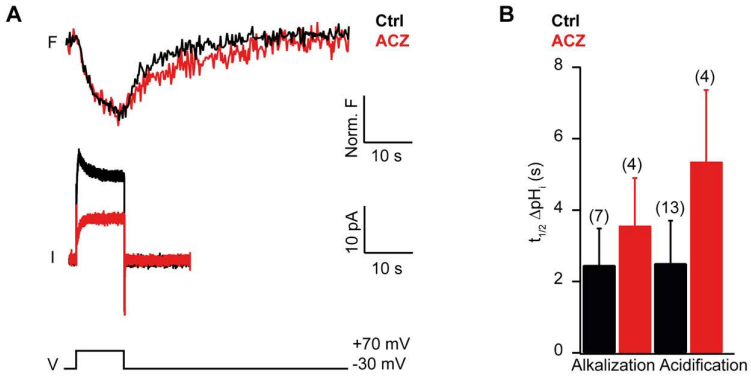

Figure 22. CA partially contributes to reacidification after depolarization-induced alkalization. (A) Time course of alkalization and reacidification (upper) and Hv1 current (lower) during a 10 s V_m pulse without (black) and with ACZ (100 µM, red) in the presence of CO_2/HCO_3^- (5%/25 mM). pH_o = 7.35; pH_i = 6.5. (B) Half-times $t_{1/2}$ (mean ± s.d.) of Hv1-mediated alkalization and acidification for controls (black) and in the presence of ACZ (100 µM, red). Several depolarizations per cell; number of cells indicated in parentheses.

The increase of fluorescence can be explained in two ways: either as diffusion of dye into the cell (e.g., after the break-in), or as intracellular acidification. The diffusion of dye from the pipette into the cell, however, takes place with a $t_{1/2}$ of <2 minutes ($t_{1/2head}$ = 69 ± 42 s, $t_{1/2flag}$ = 106 ± 52 s; Figure 8), which is slower than the observed pH_i change. The increase of fluorescence after repolarization, therefore, represents intracellular reacidification, partially due to CA activity (Figure 22B). These observations suggest that the $CO_2 + H_2O \leftrightarrow HCO_3^- + H^+$ system plays a main role in buffering pH_i in human sperm and redistribution of dye from pipette into the cell is not the major reason for the changes in fluorescence in PCF experiments.

PCF experiments of hHv1-expressing CHO cells showed similar results. The reacidification after switching back to -30 mV has a similar time course as the CO_2/HCO_3^--induced acidification (Figure 23A). Further, the depolarization-induced outward current is faster than the accompanying alkalization (Figure 23B). In contrast to sperm, it was not possible to depolarize the cells long enough to saturate the alkalization. Figure 23B shows a 4 s voltage pulse that induced a strong outward proton current (red trace), that quickly saturated. The accompanying alkalization (black trace) was slower than the current and strongly increased during the whole depolarization. The density of heterologously expressed hHv1-channels in CHO cells is likely higher than the density of the natively expressed protein in sperm. Furthermore,

human sperm harbor Hv1Sper, the isoform sensing the absolute pH, in addition to the normal hHv1 (Berger et al., 2017), which distinguishes them from the hHv1-CHO cells. The reacidification however, was 10-fold slower compared to sperm ($t_{1/2ac}$ = 32.2 ± 7 s, n_{cells} = 3, Figure 23C). The reason for this is probably the lack of CA activity and the strong acidification caused by activation of overexpressed Hv1.

In summary, these experiments highlight the importance of readjustment of the $CO_2/HCO_3^-/H^+$ equilibrium via CA and the fast diffusion of CO_2 across the cell membrane for the regulation of pH_i in sperm.

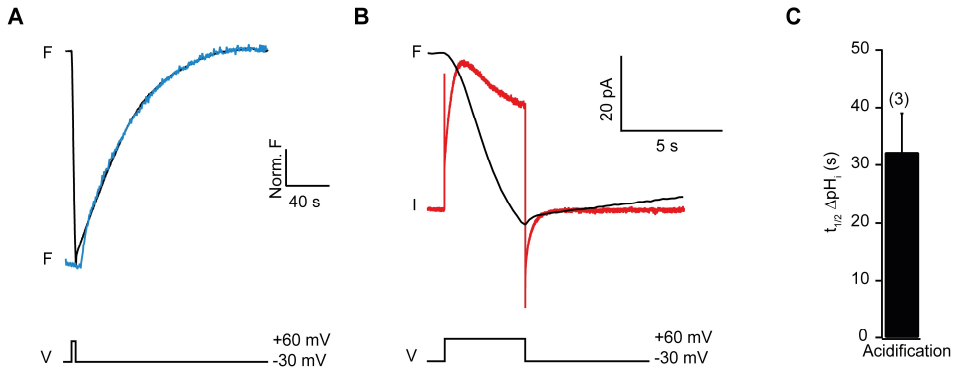

Figure 23. hHv1-CHO cells alkalize during depolarization and reacidify after repolarization but on a different time scale than sperm. (A) Superposition of the time course of normalized acidification during exposure of a hHv1-CHO cell to CO_2/HCO_3^- (5%/25 mM; blue) or termination of the V_m pulse (black) during a PCF experiment, similar to Figure 21B. pH_o = 7.35; pH_i = 6.5. Traces origin from different cells. (B) Superposition of the time course of normalized fluorescence (black) and current (red) of the patch-clamped hHv1-CHO cell from panel (A) during a voltage step from -30 mV to +60 mV. (C) Half-time $t_{½}$ (mean ± s.d.) of re-acidification in CHO-hHv1 cells after Hv1 activation (n_{cells} = 3).

3.3 pH-dependent $[Ca^{2+}]_i$ response

The ability of sperm to fertilize the oocyte is linked to pH in two ways: first, alkalization activates CatSper, leading to an increase of the intracellular Ca^{2+} concentration (Lishko et al., 2011; Strünker et al., 2011); second, HCO_3^- activates cAMP production via sAC (Chen et al., 2000). Both Ca^{2+} and HCO_3^- are crucial for the hyperactivated flagellar beating and successful fertilization (Carlson et al., 2007; Wennemuth et al., 2003). I examined the effect of pH and HCO_3^- on the calcium concentration in single non-capacitated sperm.

First, I stimulated CalBryte520-loaded sperm with the CatSper activator progesterone to serve as a positive control and to gauge incubation time and concentration of the dye. Previous studies mostly recorded progesterone responses from populations (Strünker et al., 2011) and hence might mask a possible heterogeneity between sperm.

Figure 24 shows a representative selection of single-cell calcium responses to 0.5 µM progesterone. The responses varied in shape and amplitude but were mostly transient as previously reported (Strünker et al., 2011). Surprisingly, the response had a latency of 14.2 ± 4.1 s (n_{cells} = 37, n_{exp} = 7) in contrast to the almost instantaneous progesterone responses reported by Strünker et al. (2011). The mixing time of the bath chamber is in the range of seconds (Alexa488: $\tau_{wash\text{-}in}$ = 3.1 ± 0.9 s, $\tau_{wash\text{-}out}$ = 4.1 ± 3.6 s; n_{exp} = 4; Figure 15C, D) and cannot account for the latency of the $[Ca^{2+}]_i$ increase.

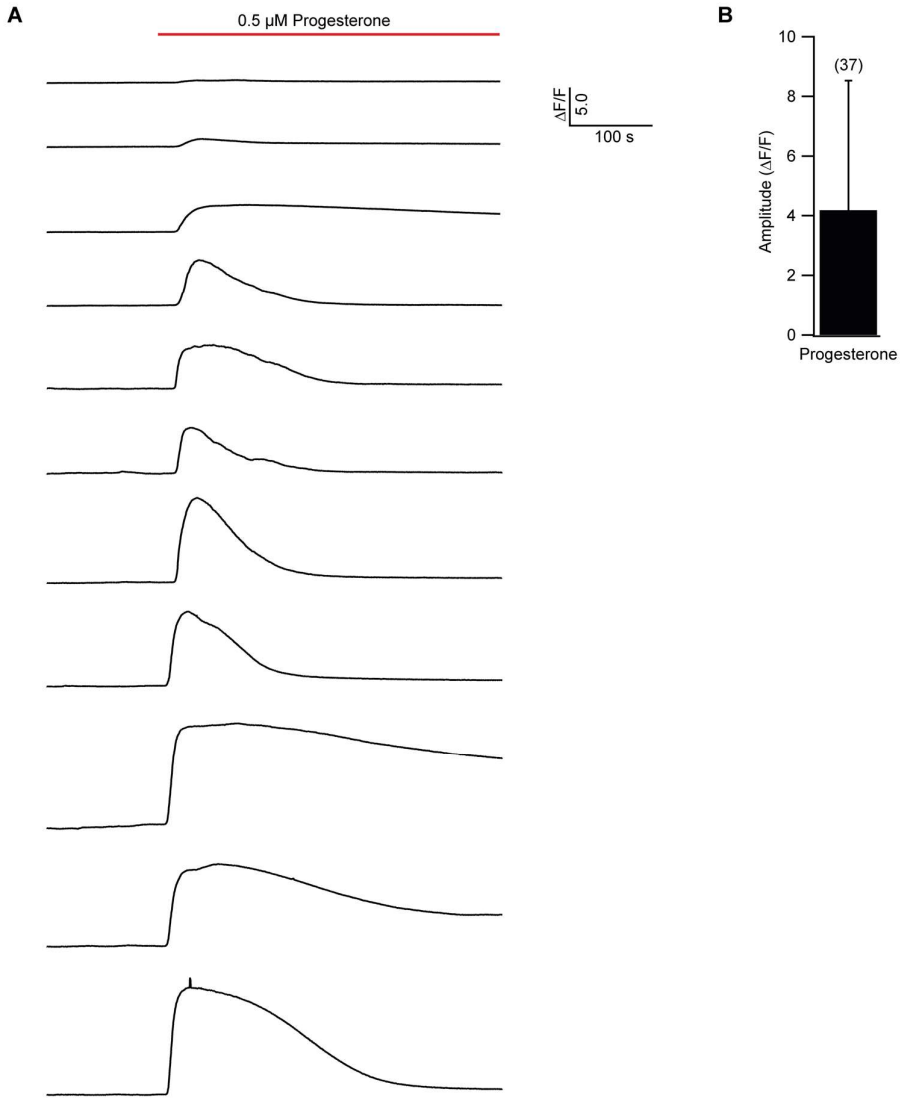

Figure 24. Representative $[Ca^{2+}]_i$ responses upon exposure to progesterone. (A) Different single-cell $[Ca^{2+}]_i$ changes upon exposure to 0.5 µM progesterone. (B) Amplitude of progesterone-induced $[Ca^{2+}]_i$ responses (mean ± s.d.; n_{exp} = 7, n_{cells} = 37).

Next, I monitored $[Ca^{2+}]_i$ while exposing sperm to a pH_o change from 6.5 to 7.7, conditions that lead to slow alkalization and might induce opening of CatSper (Figure 7A). This idea is based on sea urchin sperm, which respond with a calcium increase 200-500 ms after alkalization (Seifert et al., 2015; Strünker et al., 2011). In human sperm, however, $[Ca^{2+}]_i$ decreased with kinetics that closely followed the slow alkalization (Figure 25). While CatSper opens at alkaline pH_i, this result illustrates that a slow rise of pH_i is not sufficient for CatSper activation.

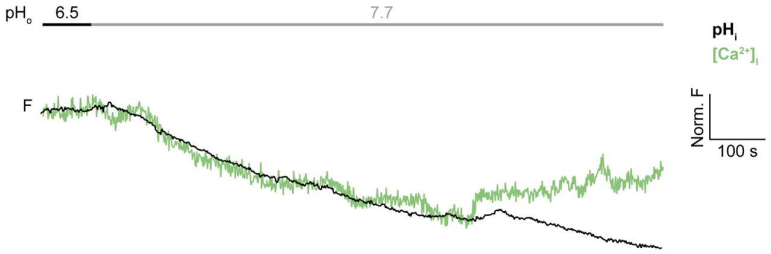

Figure 25. Increase of pH_i following pH_o does not induce a calcium response. Superposition of the fluorescence change of pHrodo-Red (black) and CalBryte520 (green) in two different sperm cells upon a switch from pH_o 6.5 to pH_o 7.7.

Because CO_2 diffusion and the subsequent conversion to HCO_3^- + H^+ by CA is the main source of HCO_3^- production in human sperm, I further examined the signaling cascade by testing if CO_2/HCO_3^- and the accompanying acidification triggers a change in $[Ca^{2+}]_i$. HCO_3^- activates sAC and increases the cAMP level in human sperm and is necessary for the capacitation. It is unclear, however, if HCO_3^- activates CatSper via the cAMP/PKA pathway, via HCO_3^--induced hyperpolarization, or not at all (Carlson et al., 2007; Orta et al., 2018; Ren et al., 2001; Seifert et al., 2015; Wang et al., 2020). During exposure and removal of CO_2/HCO_3^-, the cell response was heterogeneous (Figure 26). I categorized the responses upon exposure into the following classes: 1) no response; 2) step-like increase; 3) transient increase ("ON responses"; Figure 26A-C left). Approximately 4% of cells showed no response (1). Out of 387 cells, 68% responded with a small, step-like increase of $[Ca^{2+}]_i$ that persisted for the time of stimulation (2). Another 27% of cells displayed a transient signal that either recovered completely or declined within 100 s to a lower plateau or to baseline level. The transient signals varied in amplitude by up to 28-fold but, on average, were larger than the step-like $[Ca^{2+}]_i$ responses (Figure 26D). The responses upon removal of CO_2/HCO_3^- (OFF response) could be categorized in a similar fashion: 1) no response; 2) step-like decrease; 3) transient increase. Out of 320 cells, 7% of the cells showed no

response (1), 54% showed a step-like decrease (2), 32% of the cells showed a strong transient increase (3; Figure 26A-C right). 7% of the cells died during exposure. The transient OFF responses had slightly larger amplitudes than the ON responses, were more variable in shape, and larger than the step-like OFF responses (Figure 26E). The amplitude distribution of ON and OFF responses was similar (Figure 26D, E).

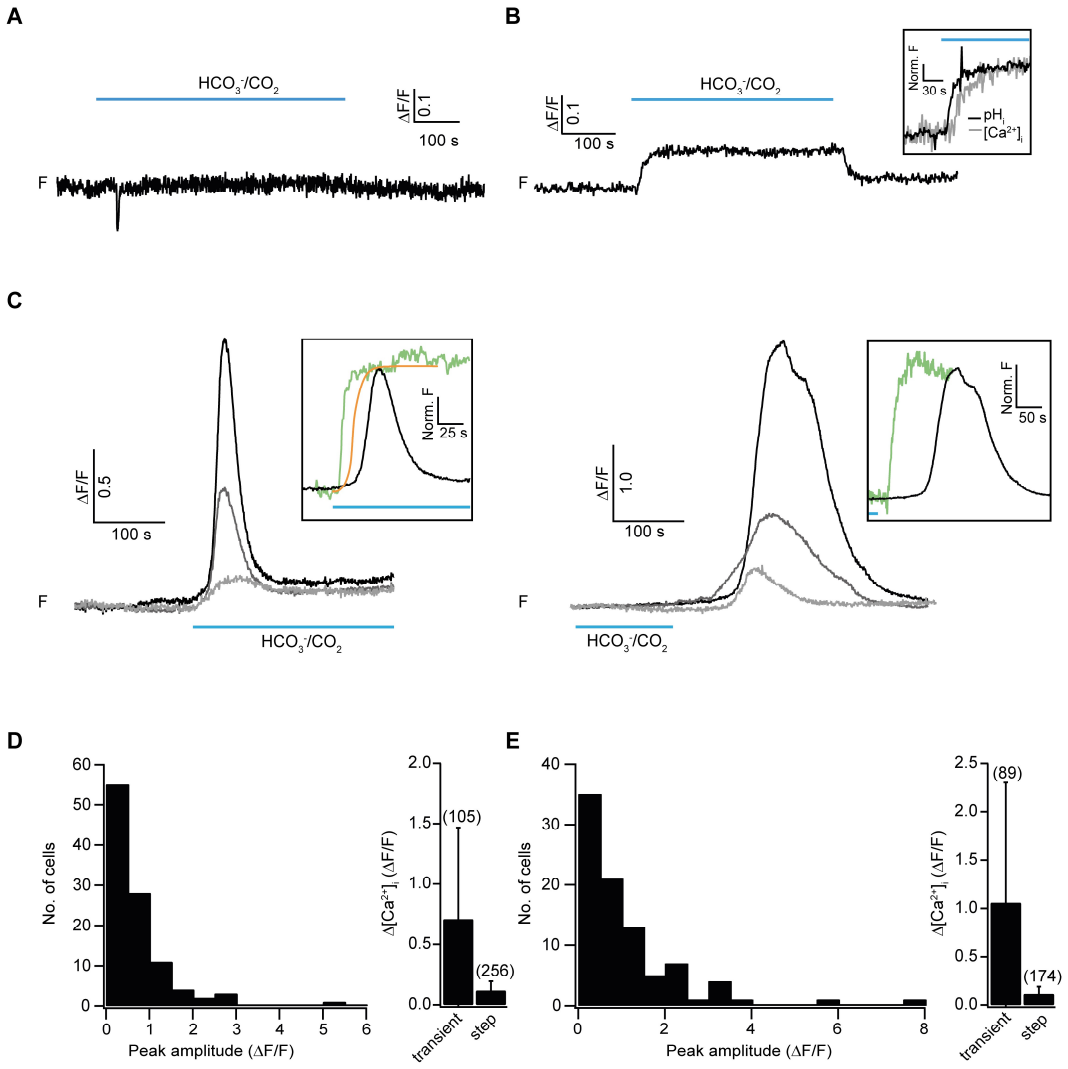

Figure 26. HCO_3^- evokes a $[Ca^{2+}]_i$ response at acidification conditions. (A-C) $[Ca^{2+}]_i$ changes of CalBryte520-loaded sperm upon switching the bath from pH_o 7.35 to pH_o 7.35/CO_2/HCO_3^- or vice versa; (A) no reaction, (B) small step-like in- and decrease, and (C) transient increase with different amplitudes upon exposure (ON, left) or removal (OFF, right) to CO_2/HCO_3^- (5%/25 mM). Insets show magnified responses superimposed onto the pH_i signal (green) and the cAMP increase (orange; Mukherjee et al., 2016). The pH_i signal on the right panel was flipped horizontally. (D, E) Histograms (left) displaying the variability of transient response amplitudes and bar graphs (right) displaying the amplitudes of transient and step-like responses to exposure (D) or removal (E) of CO_2/HCO_3^-.

The fact that a calcium response is triggered under acidifying conditions was surprising. Likewise, the heterogeneity of the responses was unexpected. Sperm acidify

uniformly within seconds after exposure to CO_2/HCO_3^- (Figure 15), I therefore expected a shorter latency and less heterogeneity of the calcium response. The inset in Figure 26C shows an example trace of the CO_2/HCO_3^--induced acidification (green) and in addition the time scale of cAMP rise caused by HCO_3^- stimulation (orange; from Mukherjee et al., 2016). The calcium response is therefore delayed until the process of acidification and cAMP increase are almost completed. So far, it is known that CatSper opens at high pH_i (Lishko et al., 2011; Strünker et al., 2011). Even if only 27% of the cells display a transient ON response, this results show that CatSper is able to open under acidifying conditions.

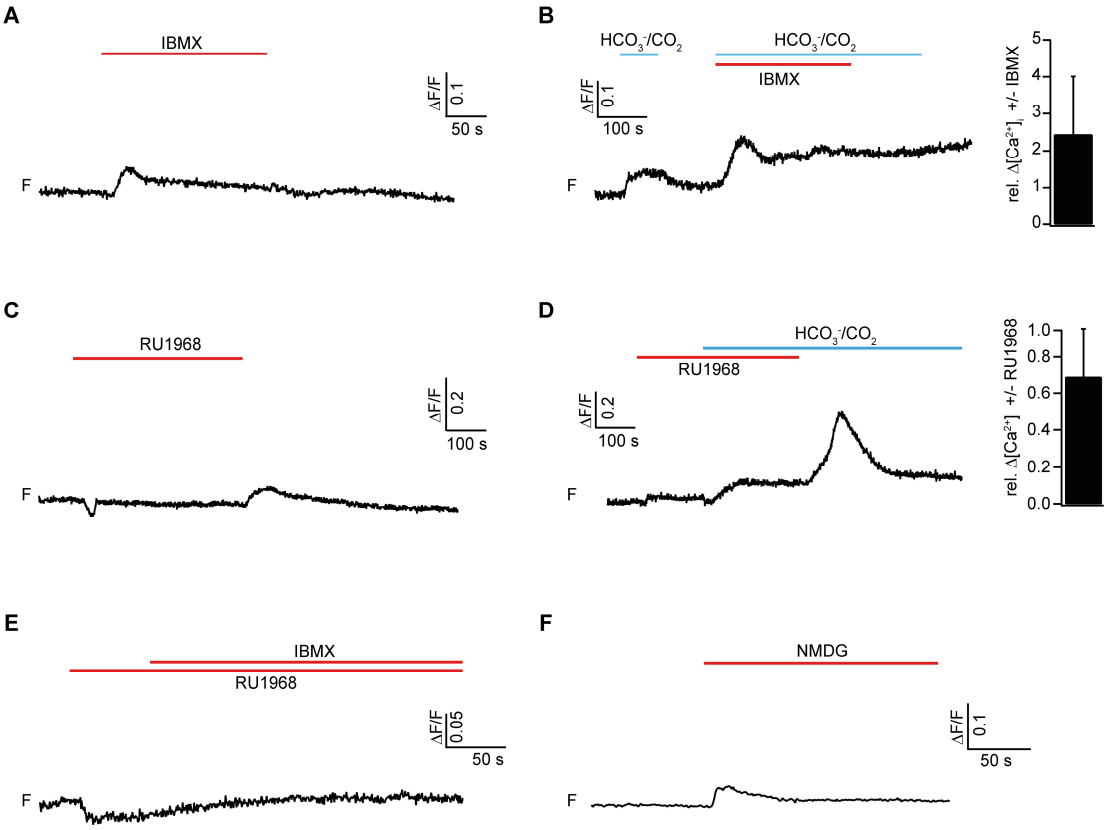

Figure 27. Pharmacology of the $[Ca^{2+}]_i$ response. (A) $[Ca^{2+}]_i$ changes of one cell upon exposure to PDE inhibitor IBMX (200 µM). (B) $[Ca^{2+}]_i$ changes of one cell upon switching the bath from pH_o 7.35 to pH_o 7.35/CO_2/HCO_3^- (5%/25 mM) and vice versa and subsequent exposure to 200 µM IBMX with CO_2/HCO_3^-. Bar graph shows the relative amplitude of $[Ca^{2+}]_i$ changes in presence of IBMX. (C) $[Ca^{2+}]_i$ changes upon exposure to CatSper inhibitor RU1968 (15 µM). (D) $[Ca^{2+}]_i$ changes upon exposure to 15 µM RU1968 and subsequent exposure to CO_2/HCO_3^- in the presence of RU1968. Bar graph shows the relative amplitude of $[Ca^{2+}]_i$ changes in presence of RU1968. (D) $[Ca^{2+}]_i$ changes upon exposure to 15 µM RU1968 and subsequent exposure to 200 µM IBMX. (F) $[Ca^{2+}]_i$ changes upon switching from Na^+-based to NMDG-based (Na^+-free) solution.

When exposing sperm to IBMX, a PDE inhibitor, $[Ca^{2+}]_i$ increases transiently (Figure 27A). IBMX inhibits the hydrolysis of cAMP and, as a consequence, increases cAMP and might promote phosphorylation of CatSper. Furthermore, when combining

IBMX with CO_2/HCO_3^-, resulting in an increased cAMP production and simultaneous inhibition of cAMP hydrolysis, the calcium response is larger in presence of the inhibitor compared to CO_2/HCO_3^- stimulation alone (Figure 27B). Upon exposure and removal of CatSper inhibitor RU1986 (Rennhack et al., 2018), sperm showed a small and diverse calcium signal (Figure 27C). Sperm exposed to CO_2/HCO_3^- in presence of RU1968, show only a slight increase in $[Ca^{2+}]_i$, but a larger transient response when RU1986 is removed but CO_2/HCO_3^- stayed constant (Figure 27D). The transient response might be a combination of the response to the inhibitor itself and the opening of already phosphorylated channels due to sAC and PKA activity. In presence of RU1986, IBMX did not evoke a $[Ca^{2+}]_i$ response (Figure 27E), suggesting that CatSper is sufficiently blocked and does not open in response to increasing cAMP. I also examined $[Ca^{2+}]_i$ in terms of regulation by a Na^+/Ca^{2+} exchanger. In sea urchin, next to the guanylate cyclase (GC), the $Na^+/Ca^{2+}/K^+$ exchanger (NCKX) is the second most abundant membrane protein (Trötschel et al., 2020) but the human sperm proteome lacks a NCKX homologue. I exposed Calbryte520-loaded sperm to a Na^+-free, NMDG-based solution. In sea urchin sperm, this induces a strong increase in $[Ca^{2+}]_i$ due to the changed ion gradient and the inward directed driving force for Ca^{2+} (Su and Vacquier, 2002). In human sperm, the solution exchange led only to a small transient increase, which suggests that $[Ca^{2+}]_i$ regulation is not Na^+-dependent and human sperm do not possess a Na^+/Ca^{2+} exchange mechanism.

Finally, I performed experiments with sperm of an infertile donor with a deletion of the CatSper2 gene that renders the channel non-functional (CatSper2$^{-/-}$; Avidan et al., 2003; Schiffer et al., 2020; Zhang et al., 2007). Overall, these cells had 3-fold lower basal $[Ca^{2+}]_i$ levels, which lead to lower signal-to-noise ratios for the calcium measurements. Exposure to CO_2/HCO_3^- did not result in a change in $[Ca^{2+}]_i$ (Figure 28A, B). As a control, the calcium ionophore ionomycin caused a strong increase of CalBryte520 fluorescence. Recording pHrodo-Red-labeled CatSper2$^{-/-}$ sperm during exposure to CO_2/HCO_3^- showed the fast acidification similar to sperm of healthy donors (Figure 28C).

Overall, the calcium responses in human sperm, independent of the stimulation, were highly variable, therefore conclusions should be considered as preliminary and taken with a grain of salt. The fact that a Ca^{2+} response can be triggered at acidic pH_i is a novel finding and should be investigated in greater detail in future experiments.

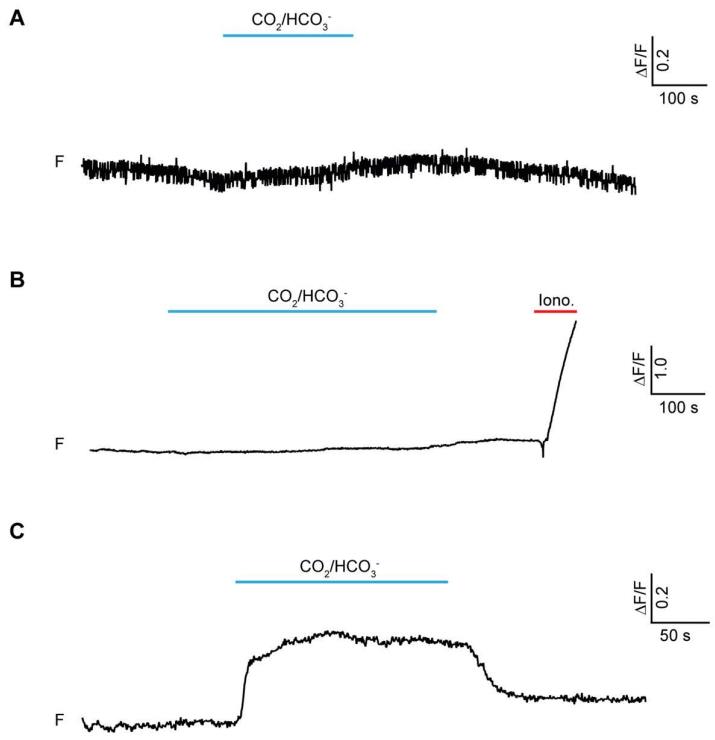

Figure 28. $[Ca^{2+}]_i$ and pH_i response of human CatSper$^{-/-}$ sperm. (A) $[Ca^{2+}]_i$ response upon exposure and removal of CO_2/HCO_3^- (5%/25 mM). (B) $[Ca^{2+}]_i$ response upon exposure and removal of CO_2/HCO_3^- and exposure to 0.5 µM ionomycin. (C) pH_i response upon exposure and removal of CO_2/HCO_3^-.

3.4 Revised human proteome

To validate the molecular identity of the players of pH regulation in human sperm, a proteome of human sperm was established in collaboration by the mass spectrometry facility at Göttingen University and the Max-Planck-Institute for Biophysical Chemistry (Svenja Kaufmann in Henning Urlaub's lab; Grahn et al., 2023). More than 4,000 proteins were identified. Among these, we searches for proteins that are directly or indirectly involved in Ca^{2+}, Na^+, HCO_3^-, H^+, or Cl^- transport, and in Ca^{2+} or cAMP signaling (Table 10; methods described in Trötschel et al., 2020). Six of these proteins are directly involved in pH regulation (HVCN1, SLC9C1&2, SLC9B1&2, SLC26A3). Furthermore, we searched for proteins that serve sperm-specific functions such as acrosomal exocytosis, axonemal proteins, or recognition between gametes (Table 11). Surprisingly, several proteins that have been proposed to be involved in ion transport, and were detected in other mass spectrometric proteomic data sets (Amaral et al., 2014; Baker et al., 2013; Gu et al., 2011; Wang et al., 2013), e.g., SLC4, CFTR, ENaC, Na^+/Ca^{2+}, or $Na^+/Ca^{2+}/K^+$ exchangers, were not detected (Table 12). The single-cell fluorometric experiments showed no functional evidence for HCO_3^- transport, which is

in agreement with the absence of potential HCO_3^- channels and exchangers. In contrast however, two isoforms of the potentially voltage-gated Na^+/H^+ exchanger sNHE, SLC9C1 and SLC9C2, were detected but their function could not be recorded with PCF. The detection limit of the mass spectrometric analysis was about 0.1 femtomolar, which is equivalent to ~60 molecules/sperm. For comparison, the copy numbers of the 11 signaling proteins of the chemotactic pathway of sea urchin sperm are 33 to 6,700-fold larger than this threshold estimation (Trötschel et al., 2020). Hence, undetected proteins either exist in very low copy numbers, or were missed. All sperm-specific proteins are found though, including all nine CatSper subunits (Table 10), suggesting that the new proteomic data to be a reliable and valuable source. The relative abundance of some of the signaling proteins identified with MS is displayed in Figure 29.

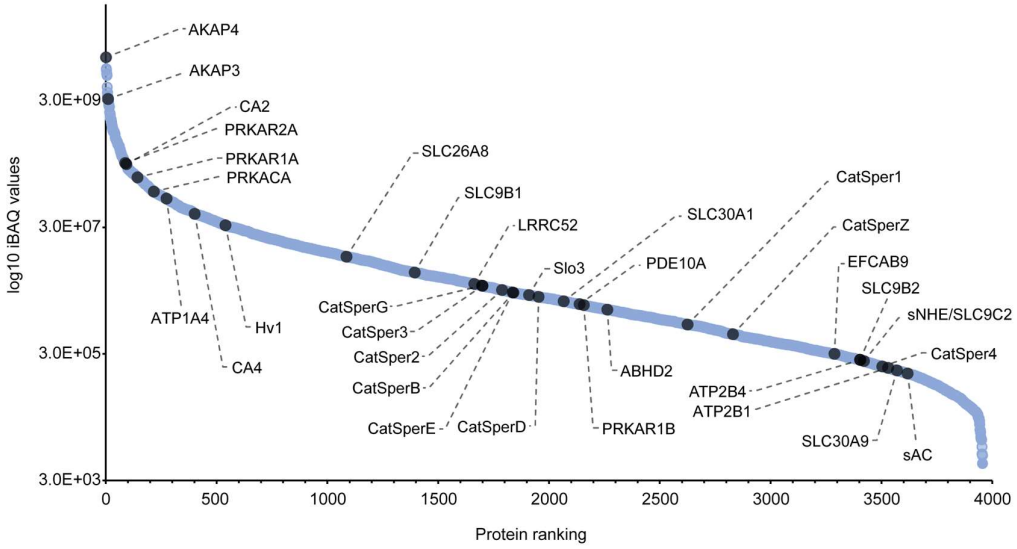

Figure 29. Ranking of signaling proteins in human sperm according to relative abundance. Abbreviations are explained in Table 10. From Grahn et al., 2023.

Table 10. Signaling proteins identified in human sperm by mass spectrometry (from Grahn et al. 2023).

Genes	Encoded proteins	Uniprot entry
ABHD2	Monoacylglycerol lipase	P08910
ADCY10	Soluble adenylate cyclase	Q96PN6
AKAP3	A-Kinase anchor protein 3	O75969
AKAP4	A-Kinase anchor protein 4	Q5JQC9
ATP1A4	Na^+/K^+-ATPase alpha-4	Q13733
ATP2B1	Plasma membrane Ca^{2+}-transporting ATPase	P20020

ATP2B3	Plasma membrane Ca^{2+}-transporting ATPase	Q16720
ATP2B4	Plasma membrane Ca^{2+}-transporting ATPase	P23634
CA 2	Carbonic anhydrase 2	P00918
CA 4	Carbonic anhydrase 4	P22748
CATSPER 1	Sperm-specific Ca^{2+} channel 1	Q8NEC5
CATSPER 2	Sperm-specific Ca^{2+} channel 2	Q96P56
CATSPER 3	Sperm-specific Ca^{2+} channel 3	Q86XQ3
CATSPER 4	Sperm-specific Ca^{2+} channel 4	Q7RTX7
CATSPER B	Sperm-specific Ca^{2+} channel beta	Q9H7T0
CATSPER G	Sperm-specific Ca^{2+} channel gamma	Q6ZRH7
CATSPER D	Sperm-specific Ca^{2+} channel delta	Q86XM0
CATSPER E	Sperm-specific Ca^{2+} channel epsilon	Q5SY80
CATSPER Z	Sperm-specific Ca^{2+} channel zeta	Q9NTU4
EFCAB9	Ca^{2+}-binding protein	A8MZ26
HVCN1	H_v1 channel	Q96D96
KCNU1	Slo3 K^+ channel	A8MYU2
LRRC52	Auxiliary subunit of Slo3	Q8N7C0
PDE10A	cAMP-specific phoshodiesterase	Q9Y233
PPP1CC	Sperm-specific phosphatase	P36873
PRKACA	cAMP-dependent protein kinase catalytic subunit alpha	P17612
PRKAR1A	cAMP-dependent protein kinase type I regulatory subunit alpha	P10644
PRKAR2A	cAMP-dependent protein kinase type II regulatory subunit alpha	P13861
PRKAR1B	cAMP-dependent protein kinase type I regulatory subunit beta	P31321
SLC9C1	Na^+/H^+ exchange	Q4G0N8
SLC9C2	Na^+/H^+ exchange	Q5TAH2
SLC9B1	Na^+/H^+ exchange	Q4ZJI4
SLC9B2	Na^+/H^+ exchange	Q86UD5
SLC26A3	Cl^-/HCO_3^- transport	P40879
SLC26A8	Cl^-, oxalate, SO_4^{2-} transport	Q96RN1
SLC30A1	Zn^{2+} transport	Q9Y6M5
SLC30A9	Zn^{2+} transport	Q6PML9
SLCO6A1	organic anion transport	Q86UG4
TMEM249	CatSper auxiliary subunit	Q2WGJ8

Table 11. Other sperm-specific proteins identified in human sperm by MS (from Grahn et al. 2023).

Genes	Encoded proteins	Uniprot entry
ACR	Acrosin	P10323
CRISP1	Cystein-rich secretory protein 1	P54107
DNAH17	Dynein heavy chain 17 axonemal	Q9UFH2
GAPDH S	Sperm-specific glyceraldehyde-3-phosphate dehydrogenase	O14556
IZUMO1	Izumo sperm-egg fusion protein 1	Q8IYV9
IZUMO2	Izumo sperm-egg fusion protein 2	Q6UXV1
IZUMO3	Izumo sperm-egg fusion protein 3	Q5VZ72
IZUMO4	Izumo sperm-egg fusion protein 4	Q1ZYL8
LDHC	L-Lactate dehydrogenase c	P07864
ODF1	Outer dense fiber protein 1	Q14990
ODF2	Outer dense fiber protein 2	Q5BJF6
ODF3	Outer dense fiber protein 3A	Q96PU9
ODF3B	Outer dense fiber protein 3B	A8MYP8
PPP3R2	Calcineurin subunit B type 2	Q96LZ3
PLCZ1	Phospholipase C zeta 1	Q86YW0
SPACA1	Sperm acrosome-associated protein 1	Q9HBV2
SPACA3	Sperm acrosome-associated protein 3	Q8IXA5
SPACA4	Sperm acrosome-associated protein 4	Q8TDM5
SPACA5	Sperm acrosome-associated protein 5	Q96QH8
SPACA6	Sperm acrosome-associated protein 6	W5XKT8
SPACA7	Sperm acrosome-associated protein 7	Q96KW9
SPACA9	Sperm acrosome-associated protein 9	Q96E40

Table 12. Signaling proteins that were not detected in human sperm by MS (from Grahn et al. 2023).

Genes	Encoded proteins	Uniprot entry
CFTR	Cystic fibrosis transmembrane conductance	P13569
KCNMA1	K^+ channel Slo1	Q12791
KCNMB1	K^+ channel Slo1 beta subunit 1	Q16558
KCNMB2	K^+ channel Slo1 beta subunit 2	Q9Y691
KCNMB3	K^+ channel Slo1 beta subunit 3	Q9NPA1
KCNMB4	K^+ channel Slo1 beta subunit 4	Q86W47

LRRC26	K^+ channel Slo1 gamma subunit 1	Q2I0M4
LRRC38	K^+ channel Slo1 gamma subunit 4	Q5VT99
LRRC55	K^+ channel Slo1 gamma subunit 3	Q6ZSA7
SCNN1A	Na^+ channel ENaC subunit A	P37088
SCNN1B	Na^+ channel ENaC subunit B	P51168
SCNN1G	Na^+ channel ENaC subunit G	P51170
SLC4A1	Cl^-/HCO_3^- transport	P02730
SLC4A2	Cl^-/HCO_3^- transport	P04920
SLC4A3	Cl^-/HCO_3^- transport	P48751
SLC4A4	Na^+/HCO_3^- co-transport	Q9Y6R1
SLC4A5	Na^+/HCO_3^- co-transport	Q9BY07
SLC4A7	Na^+/HCO_3^- co-transport	Q9Y6M7
SLC4A8	Na^+/HCO_3^- co-transport	Q2Y0W8
SLC4A9	anion exchange; protein 4	Q96Q91
SLC4A10	Na^+-driven Cl^-/HCO_3^- transport	Q6U841
SLC4A11	Na^+/HCO_3^- transporter-like	Q8NBS3
SLC8A1	Na^+/Ca^{2+} exchange 1	P32418
SLC8A2	Na^+/Ca^{2+} exchange 2	Q9UPR5
SLC8A3	Na^+/Ca^{2+} exchange 3	P57103
SLC22A14	organic cation transport	Q9Y267
SLC24A2	Na^+/Ca^{2+}-K^+ exchange	Q94I40
SLC24A4	Na^+/Ca^{2+}-K^+ exchange	Q8NFF2
SLC26A1	SO_4^{2-} transport	Q9H2B4
SLC26A2	SO_4^{2-} transport	P50443
SLC26A4	Na^+-independent Cl^-/I^- transport	Q43511
SLC26A5	prestin; Cl^-, HCO_3^- transport	P58743
SLC26A6	organic/inorganic anion transport	Q9BXS9
SLC26A7	Na^+-independent anion HCO_3^- transport	Q8TE54
SLC26A9	Cl^-/HCO_3^- exchange; HCO_3^- transport	Q7LBE3
SLC26A10	Cl^-/HCO_3^- exchange	Q8NG04
SLC26A11	Na^+-independent SO_4^{2-} transport	Q86WA9

4. Discussion

Sperm maturation and swimming are controlled by intracellular signaling cascades that involve pH changes. In my thesis, I investigated pH regulation in human sperm. I characterized the molecular mechanisms that set pH_i in sperm using a combination of electrophysiological, pharmacological, and fluorescence-optical methods.

While many ion channels and transporters have been suggested to play a role in pH regulation in human sperm (reviewed by Puga Molina, et al., 2018a), I detected a functional role of only a few players. I identified two ways protons can exit sperm: first, via an amiloride-sensitive Na^+/H^+ exchanger, and second, via the proton channel Hv1. While I could not identify a transmembrane protein that mediates direct proton entry, I could, identify the mechanism that can increase the proton concentration in sperm: uncharged CO_2 diffuses over the membrane into the cell, where the carbonic anhydrase CAII catalyzes the reaction $CO_2 + H_2O \leftrightarrow HCO_3^- + H^+$ and thereby decreases pH_i. Of note, I could not detect other previously suggested pH_i-regulating mechanisms, like bicarbonate transport by CFTR or TAT1, or hyperpolarization-activated Na^+/H^+ exchange. Finally, I show that rapid changes in the CO_2/HCO_3^- equilibrium can induce profound intracellular Ca^{2+} signaling events. Together with the proteome of human sperm recently obtained by our collaborators (Urlaub Lab, MPI for Multidisciplinary Sciences, Göttingen), my functional data provide a picture of the principal mechanisms of pH_i regulation in human sperm that are likely to govern sperm functioning and fertilization.

4.1 Transmembrane proteins regulating pH_i in human sperm

Like in most cells, pH_i in sperm is coupled to the Na^+ gradient across the membrane by a Na^+/H^+ antiport. Surprisingly, the human sperm proteome does not show standard NHE exchangers of the SLC9A family, as predicted by former proteomic studies (Baker et al., 2013; Gu et al., 2011; Wang et al., 2013), but two isoforms of the sperm-specific NHE, sNHE1 and sNHE2 (SLC9C1&2), and the two isoforms of the Na^+/H^+ antiporter, NHA1 and NHA2 (SLC9B1&2; Table 1 & Table 10).

To date, little is known about sNHE in human sperm. I tested a potentially voltage-dependent Na^+/H^+ exchange by sNHE using PCF. Motivated by a study on sea urchin sNHE (Windler et al., 2018), I anticipated activation of human sNHE by hyperpolarization. However, hyperpolarization did not change pH_i in human

sperm (Figure 9). sAC was proposed to be functionally connected to sNHE, suggesting that cAMP produced by sAC might bind to the sNHE's CNBD and subsequently activate the exchanger (Romero and Nishigaki, 2019; Wang et al., 2007). Simultaneous hyperpolarization and activation of sAC by HCO_3^- did not change pH_i neither (Figure 14). Key amino acids important for Na^+- and cyclic nucleotide-binding are not conserved in human sNHE (Windler et al., 2018). Thus, sNHE might serve a purpose different from Na^+/H^+ exchange in human sperm. Interestingly, the sNHE mouse knockout is infertile but can be rescued by increasing the intracellular cAMP concentration, suggesting a functional coupling between sAC and sNHE (Jansen et al., 2015). Recently, Cavarocchi et al. (2021) investigated sperm of an infertile man with a homozygous splicing mutation in the SLC9C1 gene that results in the deletion of the CNBD. The "truncated" protein was nevertheless expressed along the whole flagellum. Sperm had normal morphology but reduced progressive motility. Sperm ultrastructure, analyzed by electron microscopy, revealed a structurally disorganized midpiece with an excess of residual cytoplasm. The authors concluded that the mutation might cause a malfunction of the proposed functional complex of sNHE/CatSper/sAC resulting in an impaired cAMP/PKA pathway (Cavarocchi et al., 2021). Unfortunately, no further experiments, e.g., changing intracellular cAMP concentration, a motility rescue with NH_4^+ or cAMP analogues, or induction of calcium responses with progesterone were conducted to clarify the functional role of sNHE. Possibly, sNHE might only play a role in human spermatogenesis and lack function in mature sperm. Sperm displaying structural anomalies in the midpiece caused by mutation in the SLC9C1 gene suit the idea that sNHE is (also) important for spermatogenesis.

Apart from sNHE, several classic Na^+/H^+ exchangers were proposed to regulate pH_i in human sperm. Former sperm proteomes include members of the SLC9A family, which are ubiquitously expressed in the human body (Pedersen and Counillon, 2019), but were not detected in the recent proteomic analysis. Previous proteomic studies might suffer from contamination of the sperm sample with somatic cells due to the chosen preparation method. In most previous studies, sperm samples were purified using Percoll gradient centrifugation with different densities (Amaral et al., 2014; Baker et al., 2013; Wang et al., 2013). In contrast, we used the swim-up method to select for healthy sperm. The advantage of this method is that motile and healthy sperm, which

"swim up" in the HTF buffer, can be reliably separated from residual cells, such as somatic cells, immune cells, and immotile and dead sperm, which accumulate at the bottom of the vial.

I tested human sperm for functional Na^+/H^+ exchange using different experimental approaches. After induction of intracellular acidification using the acid-load technique, pH_i recovers in a Na^+-dependent and amiloride-sensitive manner (Figure 6). When exposing sperm to a higher pH_o, pH_i slowly follows pH_o. This process is also amiloride-sensitive (Figure 7A). The identity of the protein mediating this pH_i change is unclear. In human NHA1 and NHA2, the critical amino acid residues for Na^+-binding and exchange activity are conserved (Matsuoka et al., 2022). Electroneutral Na^+/H^+ exchange by NHA2 was demonstrated before (Xiang et al., 2007), the substrates and transport kinetics for NHA1 however, remain unknown. Interestingly, the NHA1 homologue of the fruit fly *D. melanogaster* was suggested to act as a H^+/Cl^- cotransporter instead of a Na^+/H^+ antiporter (Chintapalli et al., 2015). Human NHA2 (Xiang et al., 2007) and *D. melanogaster* NHA1 (Chintapalli et al., 2015) are insensitive to amiloride. For human NHA1, the amiloride sensitivity is unknown.

Altogether, the results leave room for speculation and highlight the necessity for more experiments. Especially the heterologous expression of the human sNHE1&2 and NHA1&2 would help to study the potential function of the proteins in a cellular expression system more accessible than sperm. My data show that human sperm possess at least one Na^+-dependent pH-regulator which is sensitive to amiloride. The most likely candidate for this is NHA1.

Hv1 has been identified in a previously published human sperm proteome (Wang et al., 2013) and Hv1-mediated proton currents were recorded using the patch-clamp technique (Berger et al., 2017; Lishko et al., 2010). Hv1 exclusively opens at V_m values positive to the Nernst potential for protons – therefore, Hv1 can only extrude protons and thus increase pH_i (Berger et al., 2017) and was suggested to alkalize sperm during capacitation (Lishko et al., 2010). Yet, the physiological role of Hv1 in male gametes remained enigmatic because Hv1 opening depends on both V_m and ΔpH (Berger et al., 2017; Cherny et al., 1995) and it is not known if conditions in the female reproductive tract allow sperm to reach a Vm which is sufficient for Hv1 opening (Florman et al., 2010). I measured Hv1-mediated outward currents and simultaneously recorded the depolarization-induced alkalization by PCF (Figure 9). Using this technique and single-

cell fluorometry, I aimed to shed light on a possible physiological role of Hv1 in human sperm. During depolarization, pH_i increased but saturated after a few seconds ($t_{1/2al}$ = 2.5 ± 1.0 s; Figure 21A). Hv1 currents were enhanced up to 10-fold in presence of CO_2/HCO_3^-, which acidifies the cell and therefore strongly increases the outward driving force for protons (Figure 19). After repolarization, pH_i quickly returned to the resting pH (Figure 20). Because essentially no tail current was visible during reacidification, other processes than Hv1 currents must account for pH recovery, such as HCO_3^- transport or CA activity. Further, when sperm are exposed to a higher pH_o, mimicking the environmental change from the vagina to the uterus and the oviduct, pH_i slowly follows pH_o in absence or presence of zinc, suggesting that Hv1 activity does not significantly contribute to this slow alkalization (Figure 7). Hv1 currents are reportedly enhanced in capacitated sperm (Lishko et al., 2010; Riffo et al., 1992). Unfortunately, it could not yet be determined if Hv1 currents are enhanced to induce capacitation, or *vice versa* if capacitation causes enhancement of Hv1 currents (Lishko et al., 2010).

Overall, these data suggest that Hv1 can only transiently alkalize sperm and is not involved in readjusting pH_i following the increasing pH_o. Recently, albumin was suggested to act as an Hv1 activator (Zhao et al., 2021). Interestingly, the albumin concentration is low in the seminal fluid (~15 µM; Elzanaty et al., 2007) and high in the uterus (500 µM; Casslén & Nilsson, 1984). Uterine albumin concentration increases Hv1 currents ~6-fold at +60 mV and shifts the $V_{1/2}$ to more negative potentials, suggesting that opening probability would increase in the uterus (Zhao et al., 2021). Because the high albumin concentration promotes Hv1 activation, Hv1 might alkalize the cell and subsequently increase the open probability of the alkaline-activated CatSper channel. In vitro, already 75 µM albumin, a much lower concentration than in the uterus, led to an increase in pH_i (Zhao et al., 2021). I showed that sperm possess a functional Na^+/H^+ exchanger, which exchanges ions along their gradient (Figure 6 & Figure 7). In case of a higher pH_o, as in the uterus, Na^+/H^+ exchange slowly alkalizes sperm. It remains to be determined why sperm possess two transmembrane proteins involved in acid extrusion. Possibly, this, at first glance redundant arrangement, could ensure that sperm alkalization in the female reproductive tract is not only coupled to a single but rather multiple parameters including ionic gradients (Na^+, H^+), membrane potential, and ligands like albumin. Of note, epithelial cells often

feature a combination of proton pathways across the apical or basal membrane, e.g., Na^+/H^+ exchangers and H^+ pumps (Giebisch et al., 2017).

Apart from the idea that Hv1 alkalizes the whole cell, Hv1 might be suited to regulate pH_i on a spatially more restricted level and, thereby, lead to local activation of individual CatSper channels. CatSper was found to be expressed in evenly distributed quadrilateral lines (Chung et al., 2017), whereas Hv1 dimers are expressed in bilateral lines along the flagellum (Miller et al., 2018). The distance between two Hv1 dimers on a cross-section plane is ~230 nm, which is smaller than the flagellum diameter (555-570 nm; Miller et al., 2018), resulting in Hv1 "stripes" that are "sequestered to one side of the flagellar midline" and have unequal distances to the CatSper "stripes" (Miller et al., 2018). Hv1 was suggested to induce local alkalization in the membrane area surrounding the channel, and thereby increase the open probability of CatSper channels in the close proximity (3-5 nm) of an Hv1 dimer. As a consequence, the CatSper channels on one cross-section plane are activated in an asymmetric fashion, resulting in the subsequent asymmetric increase of calcium along the flagellum. This mechanism was proposed to be responsible for the "rotational" flagellar movement of sperm (Miller et al., 2018). Thus, Hv1 might not set resting pH_i (which is achieved by amiloride sensitive Na^+/H^+ exchange) but rather serve as a proton exit valve that is only briefly active at a depolarized membrane potential in combination with local drop in pH_i. Consequently, the locally restricted proton extrusion might activate adjacent CatSper channels in an asymmetric fashion. While this concept is somewhat speculative, it would be nevertheless interesting to investigate whether the Na^+/H^+ exchanger in human sperm is also arranged in such a particular pattern. Several aspects of the function of Hv1 in human sperm remain to be clarified; a patient with Hv1 impairment would help to shed light on the channel's importance for male fertility.

Table 13. Putative pH-regulating proteins validated by mass spectrometry.

Protein	Wang et al., 2013	Baker et al., 2013	Amaral et al., 2014	Gu et al., 2011	Grahn et al., 2023
CA II	✓				✓
CA IV	✓		✓		✓
CFTR				✓	
SLC4A1 (AE1)	✓				

SLC4A3 (AE3)				✓	
SLC4A5 (NBC)				✓	
SLC26A8	✓		✓		✓
SLC9A1	✓				
SLC9A2				✓	
SLC9A3		✓			
SLC9A5				✓	
SLC9A9				✓	
SLC9B1					✓
SLC9B2					✓
SLC9C1	✓				✓
SLC9C2					✓
HVCN1 (Hv1)	✓				✓

✓ = detected in mass spectrometric data.

4.2 The $CO_2 + H_2O \leftrightarrow HCO_3^- + H^+$ equilibrium and capacitation

HCO_3^- is the most important non-proteinaceous pH buffer; in addition, HCO_3^- is an intracellular messenger and a key factor of fertilization in sperm: HCO_3^- activates sAC, which in turn produces cAMP (Rahman et al., 2013). For decades, HCO_3^-, which is present at high concentrations in the female reproductive, was thought to enter sperm via transporters or exchangers (reviewed by De Jonge, 2017; Puga Molina, et al., 2018a; Visconti et al., 2011). I investigated the dependence of pH_i on extracellular HCO_3^- in human sperm and showed that CO_2 diffusion over the membrane and intracellular conversion to $HCO_3^- + H^+$ by CAII is faster than a putative HCO_3^--transport. In agreement, mass spectrometric data suggests that CAII is one of the most abundant proteins in human sperm (Figure 29).

Exposure to CO_2/HCO_3^- decreased pH_i in human sperm (Figure 15). This can be explained by CO_2 diffusion across the membrane with a predicted permeability P_{CO2} between $1.5x10^{-3}$ cm/s and 0.33 cm/s (Endeward et al., 2017). Inside of the cell, the reaction $CO_2 + H_2O \leftrightarrow HCO_3^- + H^+$ is quickly catalyzed by CAII, and protons acidify the cell. Conversely, transport of HCO_3^- into the cell would induce alkalization, an argument which is generally used to explain the pH_i increase during *in-vitro* capacitation (reviewed by De Jonge, 2017; Puga Molina, et al., 2018a; Visconti et al., 2011) but is not in line with my data. Furthermore, I showed that inhibition of putative

HCO_3^- transporters did not alter ΔpH_i or $\tau_{\Delta pHi}$ during CO_2/HCO_3^- exposure, suggesting that HCO_3^- transport is either too slow to have an impact on ΔpH, or is absent (Figure 16). In addition, we identified the CAIV isoform in the human sperm proteome. In mouse sperm and other cell types, CAIV is located and operating at the extracellular side of the plasma membrane. Thus, extracellular HCO_3^- might be converted to CO_2 in the vicinity of the sperm membrane, and allow rapid CO_2 diffusion into the cytosol.
Our proteomic data lacks CFTR, NBC, and putative HCO_3^- exchangers of the SLC4 family, except for TAT1 (SLC28A8; Table 12 & Table 13). A study shows that men exhibiting a mutation in the TAT1 gene are infertile and their sperm showed reduced motility (Dirami et al., 2013). Interestingly, exposing cells expressing a functional HCO_3^- transporter to CO_2/HCO_3^-, behave differently compared to human sperm: cells with functional HCO_3^- transporters also immediately acidify, but, after the initial pH_i decrease, while still being exposed to CO_2/HCO_3^-, pH_i partially recovers (Müller et al., 2000). This recovery is inhibited by DIDS by 88%. Potentially, HCO_3^-, generated by CA after CO_2 diffusion into the cell, might be extruded by a HCO_3^- transporter or exchanger. In contrast, sperm do not display a pH_i recovery during CO_2/HCO_3^- exposure (Figure 15B) and lack most of the proposed HCO_3^- transporters in the proteome (Table 1 & Table 10).

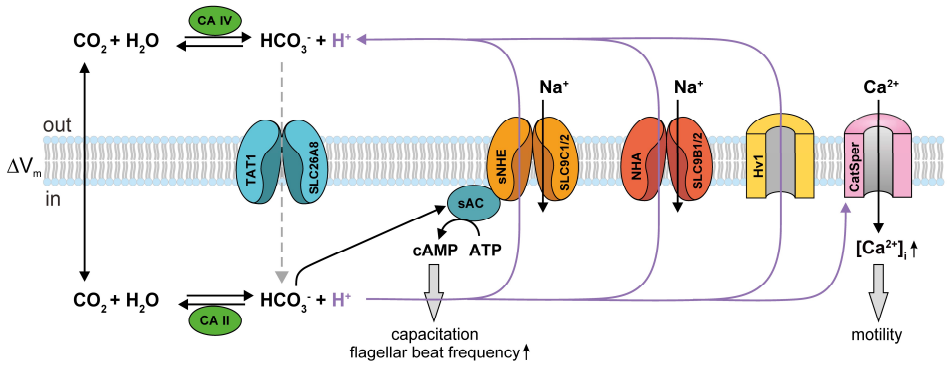

Figure 30. Putative pH-regulating proteins in human sperm validated by mass spectrometry. Protons enter the cell indirectly via CO_2 diffusions and CAII activity and might leave the cell via sNHE1/2, NHA1/2 or Hv1 (violet arrows). HCO_3^- entry via TAT1 is possible but could not be confirmed yet (dashed grey arrow).

It is worth to compare sperm with other cells displaying particular $CO_2/HCO_3^-/H^+$ handling using similar sets of proteins. Epithelial cells of the proximal tubule of the kidney reabsorb HCO_3^- from primary urine using several proteins that are also present in human sperm: at the apical, urine-facing side, HCO_3^- is converted to CO_2 by the extracellular CAIV. Following CO_2 diffusion into the cell, CAII catalyzes conversion of

CO_2 to HCO_3^- + H^+. Excessive protons are removed back into urine by Na^+/H^+ exchange, where protons can react again with HCO_3^- to further support CO_2 formation in the urine (Giebisch et al., 2017). I suggest that, to this point, the same processes happen in sperm in the female reproductive tract (Figure 30; violet arrows represent "cycle of protons"). Then, the fate of the intracellularly accumulated HCO_3^- is different between tubule cells and sperm: in tubule cells, a basolateral symporter promotes reabsorption of Na^+ and HCO_3^- into the interstitial space; in sperm, HCO_3^- serves as a second messenger to stimulate sAC to produce cAMP (Chen et al., 2000).

In my experiments, I did not find any evidence of TAT1 functioning as a HCO_3^- transporter. The protein might nonetheless play an important role in fertilization and regulation of the Cl^-/HCO_3^- equilibrium, but my data suggests that the exchanger plays only a minor role in pH regulation. For mouse sperm, Carlson et al. (2007) showed that CO_2 diffusion over the membrane and hydration to HCO_3^- is the source of intracellular HCO_3^-. They reported no pH_i change after 30 s exposure to 15 mM HCO_3^- but acceleration of flagellar beat. Inhibitors of anion exchangers (4-acetamido-4′-isothiocyanatostilbene-2,2′-disulfonic acid; SITS) and CFTR ($CFTR_{inh}$-172) did not alter the change in flagellar beat, but the presence of a CA inhibitor (ACZ) prolonged the time from ~35 s to ~60 s for sperm to reach the maximum frequency. Likewise, in my experiments, $\tau_{\Delta pHi}$ during CO_2/ HCO_3^- exposure strongly increased in presence of ACZ (from 5.6 ± 2.2 s to 38.9 ± 15 s, Figure 17C).

Because exposure to CO_2/HCO_3^- instantaneously acidifies sperm, capacitation-induced alkalization is most likely not caused by the increase in intracellular HCO_3^-. Previous reports on capacitation-induced alkalization differ in experimental methods as well as reported pH_i changes (Babcock, 1983; Carlson et al., 2007; Cross and Razy-Faulkner, 1997; Demarco et al., 2003; López-González et al., 2014; Meizel and Deamer, 1978; Nakanishi et al., 2001; Parrish et al., 1989; Vredenburgh-Wilberg and Parrish, 1995; Xu et al., 2007; Zeng et al., 1995). Some of these experiments did not use HCO_3^- to induce capacitation (Babcock, 1983; Meizel and Deamer, 1978; Parrish et al., 1989; Vredenburgh-Wilberg and Parrish, 1995) but are often cited by other researchers for HCO_3^--induced alkalization nonetheless. Several studies using HCO_3^- reported modest pH_i increases between 0.14-0.19 (Zeng et al., 1996 (mouse); Demarco et al., 2003 (mouse); Cross & Razy-Faulkner, 1997 (human)). Xu et al. (2007) reported a larger ΔpH_i of 0.75 (mouse). Carlson et al. (2007) reported no change (human). One reason

for the measured pH_i increase might be the long capacitation times (2 hours Xu et al., 2007; Zeng et al., 1996; 24 hours Cross & Razy-Faulkner, 1997; not stated in Demarco et al., 2003). Sperm were incubated in HCO_3^--containing solutions in an open system. pCO_2 is 0.3 mmHg in the atmosphere whereas pCO_2 is 40 mmHg in the human body (Boron, 2016). Exposing HCO_3^--containing solutions to the atmospheric pCO_2 leads to degassing of CO_2, resulting in slow alkalization of the solution by equilibration of the $CO_2 + H_2O \leftrightarrow HCO_3^- + H^+$ system. I showed that alkalization of the extracellular solution results in slow intracellular alkalization by Na^+/H^+ exchange (Figure 7). The measured pH_i increase might, therefore, be an artifact due to an unstable pH_o and is not the result of HCO_3^- transport into sperm.

4.3 pH-dependent $[Ca^{2+}]_i$ response

Calcium influx is a crucial step during fertilization and is mediated by CatSper. CatSper is a multimodal cation channel that opens at nanomolar concentrations of the female sex hormone progesterone and by intracellular alkalization (Lishko et al., 2011; Strünker et al., 2011). My experiments contradict common belief of intracellular alkalization due to HCO_3^- influx, therefore, I finally tested if exposing sperm to CO_2/HCO_3^- has an impact on $[Ca^{2+}]_i$. Experiments with the Ca^{2+} indicator CalBryte-520 gave rise to several interesting but in parts heterogeneous findings. After exposure to CO_2/HCO_3^-, some sperm displayed transient or step-like calcium signals under acidifying conditions (ΔpH_i = -0.11 compared to resting pH_i; Figure 26), although CatSper activation requires either an alkaline pH_i or another activator such as progesterone (Lishko et al., 2011; Strünker et al., 2011). Activation via CO_2/HCO_3^- suggests the involvement of the cAMP pathway and an intertwined regulation of CatSper via pH_i and cAMP. pH_i and cAMP are coupled via the HCO_3^--sensitive sAC. An increase in HCO_3^- upregulates cAMP production which could increase the CatSper open probability. At the same time, the extracellular presence of CO_2/HCO_3^- decreases pH_i due to the fact that CO_2 diffuses through the membrane and the reaction $CO_2 + H_2O \leftrightarrow HCO_3^- + H^+$ is catalyzed by CAII, which counteracts this process by decreasing the CatSper open probability. Recently, the possible activation of CatSper by HCO_3^- or the cAMP/PKA was discussed by T. Wang et al. (2020). The study excluded a physiological relevant CatSper activation by the cAMP/PKA pathway. However, they explained and showed that a HCO_3^--induced calcium response can be caused by

experimental artefacts: CatSper is activated by an alkaline pH_o. Exposing HCO_3^--containing solutions to air leads to a pH increase of the solution by degassing of CO_2. Consequently, exposing sperm to a HCO_3^- solution, which is not gassed with CO_2, induces false-positive calcium responses. There are a few reports showing HCO_3^--induced calcium responses but there are as well reports recording no HCO_3^--induced calcium response: Orta et al. (2018) reported a step-like calcium response, whereas Spehr et al. (2004) and Veitinger et al. (2011) reported transient calcium signals. Carlson et al. (2007) and Strünker et al. (2011) reported no calcium response. In none of these publications it is stated, if the HCO_3^- solutions were gassed with CO_2, therefore, I assume that it was neglected. Because I used pH-controlled, continually CO_2-gassed solutions for my experiments to keep pCO_2 and therefore pH constant, the calcium responses I recorded are unlikely to result from unstable pH conditions. A possible explanation for the high variability of my results might be that the CatSper channel harbors a mechanism to integrate changes in pH_i and cAMP. One part of this mechanism might be the recently identified CatSper-associated protein, EF-hand calcium-binding domain containing protein 9 (EFCAB9), which was reported to regulate pH-dependent CatSper activation in mouse sperm (Hwang et al., 2019). EFCAB9 which binds to CatSperζ and is released at alkaline pH_i (Hwang et al., 2019). In EFCAB9$^{-/-}$ sperm, CatSper activation was almost insensitive to alkaline pH_i. EFCAB9 was also detected in the human sperm proteome (Table 10). There are, however, amino-acid substitutions in the Ca^{2+}-binding cavity of EFCAB9. Of the three predicted EF motifs, which, in sea urchin, harbor a negatively charged glutamate at position 12, mouse and human express glutamine and asparagine or lysine and asparagine in EF1 and EF2, respectively (Hwang et al., 2019). The Ca^{2+} affinity might therefore not be evolutionary conserved between species.

The following model is an attempt to explain the observed phenomenon of highly variable calcium responses: one of the CatSper subunits or the associated protein EFCAB9 might exist in different phosphorylation states. The binding of Ca^{2+}-binding proteins, like calmodulin, to its target protein is frequently regulated by phosphorylation (reviewed by Yang and Tsai, 2022). The different phosphorylation states of CatSper or CatSper subunits might set apart capacitated from non-capacitated cells and may explain why only a fraction of sperm at any given time is capacitated (Cohen-Dayag et al., 1995). Whereas in the unphosphorylated state, the channel is

sensitive to pH_i and opens at alkaline pH_i, in the phosphorylated state, CatSper might lose pH sensitivity and can open at lower pH_i (Figure 31). Thus, the balance between pH_i and cAMP controls CatSper activity. Considering the variable Ca^{2+} responsiveness and previous conflicting reports about a cAMP-mediated control of CatSper (Orta et al., 2018; Wang et al., 2020) further work is required to substantiate this hypothesis.

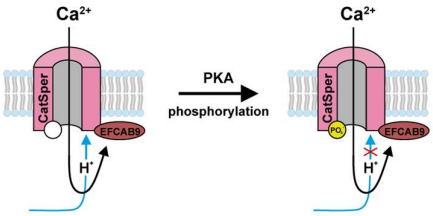

Figure 31. Regulation of CatSper by pH_i, Ca^{2+}, and cAMP. Unphosphorylated CatSper is sensitive to pH_i. Phosphorylation by PKA renders the channel insensitive to pH_i. Ca^{2+} can bind to EFCAB9. The CatSper icon has been tagged with a phosphate group; however, phosphorylation sites at other signaling components may be functionally equivalent.

5. References

Ahmad A, Ahmed A, Patrizio P. 2013. Cystic fibrosis and fertility. *Curr Opin Obstet Gynecol*.

Amaral A, Castillo J, Ramalho-Santos J, Oliva R. 2014. The combined human sperm proteome: cellular pathways and implications for basic and clinical science. *Hum Reprod Update*.

Arnoult C, Zeng Y, Florman HM. 1996. ZP3-dependent activation of sperm cation channels regulates acrosomal secretion during mammalian fertilization. *J Cell Biol*.

Aronson PS, Nee J, Suhm MA. 1982. Modifier role of internal H^+ in activating the Na^+-H^+ exchanger in renal microvillus membrane vesicles. *Nature*.

Austin CR. 1951. Observations on the penetration of the sperm into the mammalian egg. *Aust J Biol Sci*.

Avidan N, Tamary H, Dgany O, Cattan D, Pariente A, Thulliez M, Borot N, Moati L, Barthelme A, Shalmon L, Krasnov T, Ben-Asher E, Olender T, Khen M, Yaniv I, Zaizov R, Shalev H, Delaunay J, Fellous M, Lancet D, Beckmann JS. 2003. CATSPER2, a human autosomal nonsyndromic male infertility gene. *Eur J Hum Genet*.

Babcock DF. 1983. Examination of the intracellular ionic environment and of ionophore action by null point measurements employing the fluorescein chromophore. *J Biol Chem*.

Baker MA, Naumovski N, Hetherington L, Weinberg A, Velkov T, Aitken RJ. 2013. Head and flagella subcompartmental proteomic analysis of human spermatozoa. *Proteomics*.

Balbach M, Hamzeh H, Jikeli JF, Brenker C, Schiffer C, Hansen JN, Neugebauer P, Trötschel C, Jovine L, Han L, Florman HM, Kaupp UB, Strünker T, Wachten D. 2020. Molecular mechanism underlying the action of zona-pellucida glycoproteins on mouse sperm. *Front Cell Dev Biol*.

Battistone MA, Da Ros VG, Salicioni AM, Navarrete FA, Krapf D, Visconti PE, Cuasnicú PS. 2013. Functional human sperm capacitation requires both bicarbonate-dependent PKA activation and down-regulation of Ser/Thr phosphatases by Src family kinases. *Mol Hum Reprod*.

Berger TK, Fußhöller DM, Goodwin N, Bönigk W, Müller A, Dokani Khesroshahi N, Brenker C, Wachten D, Krause E, Kaupp UB, Strünker T. 2017. Post-translational cleavage of Hv1 in human sperm tunes pH- and voltage-dependent gating. *J Physiol*.

Bleil JD, Wassarman PM. 1983. Sperm-egg interactions in the mouse: Sequence of events and induction of the acrosome reaction by a zona pellucida glycoprotein. *Dev Biol*.

Boron WF. 2016. Chapter V: The respiratory system In: Boron WF, Boulpaep EL (editors). Medical Physiology. 3rd edition. *Elsevier Inc*.

Boron WF. 2004. Regulation of intracellular pH. *Am J Physiol - Adv Physiol Educ*.

Boron WF, De Weer P. 1976. Intracellular pH transients in squid giant axons caused by CO_2, NH_3, and metabolic inhibitors. *J Gen Physiol*.

Brenker C, Goodwin N, Weyand I, Kashikar ND, Naruse M, Krähling M, Müller A, Kaupp UB, Strünker T. 2012. The CatSper channel: a polymodal chemosensor in human sperm. *EMBO J*.

Brenker C, Zhou Y, Müller A, Echeverry FA, Trötschel C, Poetsch A, Xia X-M, Bönigk W, Lingle CJ, Kaupp UB, Strünker T. 2014. The Ca^{2+}-activated K^+ current of human sperm is mediated by Slo3. *Elife*.

Brown SG, Publicover SJ, Mansell SA, Lishko P V., Williams HL, Ramalingam M, Wilson SM, Barratt CLR, Sutton KA, Da Silva SM. 2016. Depolarization of sperm membrane potential is a common feature of men with subfertility and is associated with low fertilization rate at IVF. *Hum Reprod*.

Buffone MG, Wertheimer E V., Visconti PE, Krapf D. 2014. Central role of soluble adenylyl cyclase and cAMP in sperm physiology. *Biochim Biophys Acta*.

Carlson AE, Hille B, Babcock DF. 2007. External Ca^{2+} acts upstream of adenylyl cyclase SACY in the bicarbonate signaled activation of sperm motility. *Dev Biol*.

Casslén B, Nilsson B. 1984. Human uterine fluid, examined in undiluted samples for osmolarity and the concentrations of inorganic ions, albumin, glucose, and urea. *Am J Obstet Gynecol*.

Cavarocchi E, Whitfield M, Chargui A, Stouvenel L, Lorès P, Coutton C, Arnoult C, Santulli P, Patrat C, Thierry-Mieg N, Ray PF, Dulioust E, Touré A. 2021. The sodium/proton exchanger SLC9C1 (sNHE) is essential for human sperm motility and fertility. *Clin Genet*.

Chang MC. 1951. Fertilizing capacity of Spermatozoa deposited into the Fallopian tubes. *Nature*.

Chávez JC, Hernández-González EO, Wertheimer E, Visconti PE, Darszon A, Treviño CL. 2012. Participation of the Cl^-/HCO_3^- exchangers SLC26A3 and

SLC26A6, the Cl^- channel CFTR, and the regulatory Factor SLC9A3R1 in mouse sperm capacitation. *Biol Reprod*.

Chen SR, Chen M, Deng SL, Hao XX, Wang XX, Liu YX. 2016. Sodium–hydrogen exchanger NHA1 and NHA2 control sperm motility and male fertility. *Cell Death Dis*.

Chen WY, Xu WM, Chen ZH, Ni Y, Yuan YY, Zhou SC, Zhou WW, Tsang LL, Chung YW, Höglund P, Chan HG, Shi QX. 2009. Cl^- Is required for HCO_3^- entry necessary for sperm capacitation in guinea pig: Involvement of a Cl^-/HCO_3^--exchanger (SLC26A3) and CFTR. *Biol Reprod*.

Chen Y, Cann MJ, Litvin TN, Iourgenko V, Sinclair ML, Levin LR, Buck J. 2000. Soluble adenylyl cyclase as an evolutionarily conserved bicarbonate sensor. *Science*.

Cherny V V., Markin VS, Decoursey TE. 1995. The Voltage-activated hydrogen ion conductance in rat alveolar epithelial cells is determined by the pH gradient. *J Gen Physiol*.

Chintapalli VR, Kato A, Henderson L, Hirata T, Woods DJ, Overend G, Davies SA, Romero MF, Dow JAT. 2015. Transport proteins NHA1 and NHA2 are essential for survival, but have distinct transport modalities. *Proc Natl Acad Sci USA*.

Christianson DW, Fierke CA. 1996. Carbonic anhydrase: Evolution of the zinc binding site by nature and by design. *Acc Chem Res*.

Chung JJ, Miki K, Kim D, Shim SH, Shi HF, Hwang JY, Cai X, Iseri Y, Zhuang X, Clapham DE. 2017. Catsperz regulates the structural continuity of sperm Ca^{2+} signaling domains and is required for normal fertility. *Elife*.

Cohen-Dayag A, Tur-Kaspa I, Dor J, Mashiach S, Eisenbach M. 1995. Sperm capacitation in humans is transient and correlates with chemotactic responsiveness to follicular factors. *Proc Natl Acad Sci USA*.

Cross NL, Morales P, Overstreet JW, Hanson FW. 1988. Induction of Acrosome Reactions by the Human Zona Pellucida. *Biol Reprod*.

Cross NL, Razy-Faulkner P. 1997. Control of Human Sperm Intracellular pH by Cholesterol and its Relationship to the Response of the Acrosome to Progesterone. *Biol Reprod*.

David A, Serr DM, Czernobilsky B. 1973. Chemical composition of human oviduct fluid. *Fertil Steril*.

De Jonge C. 2017. Biological basis for human capacitation-revisited. *Hum Reprod Update*.

de Souza DAS, Faucz FR, Pereira-Ferrari L, Sotomaior VS, Raskin S. 2017. Congenital bilateral absence of the vas deferens as an atypical form of cystic fibrosis: reproductive implications and genetic counseling. *Andrology*.

Demarco IA, Espinosa F, Edwards J, Sosnik J, De la Vega-Beltrán JL, Hockensmith JW, Kopf GS, Darszon A, Visconti PE. 2003. Involvement of a Na^+/HCO_3^- cotransporter in mouse sperm capacitation. *J Biol Chem*.

Dirami T, Rode B, Jollivet M, Da Silva N, Escalier D, Gaitch N, Norez C, Tuffery P, Wolf J-P, Becq F, Ray PF, Dulioust E, Gacon G, Bienvenu T, Touré A. 2013. Missense mutations in SLC26A8, encoding a sperm-specific activator of CFTR, are associated with human asthenozoospermia. *Am J Hum Genet*.

Eggert-Kruse W, Köhler A, Rohr G, Runnebaum B. 1993. The pH as an important determinant of sperm-mucus interaction. *Fertil Steril*.

El Khouri E, Whitfield M, Stouvenel L, Kini A, Riederer B, Lores P, Roemermann D, di Stefano G, Drevet JR, Saez F, Seidler U, Touré A. 2018. Slc26a3 deficiency is associated with epididymis dysplasia and impaired sperm fertilization potential in the mouse. *Mol Reprod Dev*.

Elzanaty S, Erenpreiss J, Becker C. 2007. Seminal plasma albumin: Origin and relation to the male reproductive parameters. *Andrologia*.

Endeward V, Arias-Hidalgo M, Al-Samir S, Gros G. 2017. CO_2 permeability of biological membranes and role of CO_2 channels. *Membranes (Basel)*.

Fisch JD, Behr B, Conti M. 1998. Enhancement of motility and acrosome reaction in human spermatozoa: differential activation by type-specific phosphodiesterase inhibitors. *Hum Reprod*.

Flesch FM, Brouwers JFHM, Nievelstein PFEM, Verkleij AJ, Van Golde LMG, Colenbrander B, Gadella BM. 2001. Bicarbonate stimulated phospholipid scrambling induces cholesterol redistribution and enables cholestrol depletion in the sperm plasma membrane. *J Cell Sci*.

Florman HM, Jungnickel MK, Sutton KA. 2010. Shedding light on sperm pHertility. *Cell*.

Florman HM, Jungnickel MK, Sutton KA. 2008. Regulating the acrosome reaction. *Int J Dev Biol*.

Frelin C, Barbry P, Vigne P, Chassande O, Cragoe EJ, Lazdunski M. 1988. Amiloride and its analogs as tools to inhibit Na^+ transport via the Na^+ channel, the Na^+/H^+ antiport and the Na^+/Ca^{2+} exchanger. *Biochimie*.

Garcia MA, Meizel S. 1999. Regulation of intracellular pH in capacitated human spermatozoa by a Na^+/H^+ exchanger. *Mol Reprod Dev*.

Garcia MA, Meizel S. 1996. Importance of sodium ion to the progesterone-initiated acrosome reaction in human sperm. *Mol Reprod Dev*.

Giebisch G, Windhager EE, Aronson PS. 2017. Chapter VI: The urinary system In: Boron WF, Boulpaep EL (editors). Medical Physiology. 3rd edition. *Elsevier Inc*.

Grahn E, Kaufmann SV., Askarova M, Ninov M, Welp LM, Berger TK, Urlaub H, Kaupp UB. 2023. Control of intracellular pH and bicarbonate by CO_2 diffusion into human sperm. *Nat Commun*.

Gu B, Zhang J, Wu Y, Zhang X, Tan Z, Lin Y, Huang X, Chen L, Yao K, Zhang M. 2011. Proteomic analyses reveal common promiscuous patterns of cell surface proteins on human embryonic stem cells and sperms. *PLoS One*.

Hamill OP, Marty A, Neher E, Sakmann B, Sigworth FJ. 1981. Improved patch-clamp techniques for high-resolution current recording from cells and cell-free membrane patches. *Pflügers Arch - Eur J Physiol*.

Harrison RAP, Gadella BM. 2005. Bicarbonate-induced membrane processing in sperm capacitation. *Theriogenology*.

Hernández-González EO, Treviño CL, Castellano LE, De La Vega-Beltrán JL, Ocampo AY, Wertheimer E, Visconti PE, Darszon A. 2007. Involvement of cystic fibrosis transmembrane conductance regulator in mouse sperm capacitation. *J Biol Chem*.

Hess KC, Jones BH, Marquez B, Chen Y, Ord TS, Kamenetsky M, Miyamoto C, Zippin JH, Kopf GS, Suarez SS, Levin LR, Williams CJ, Buck J, Moss SB. 2005. The "soluble" adenylyl cyclase in sperm mediates multiple signaling events required for fertilization. *Dev Cell*.

Hihnala S, Höglund P, Lammi L, Kokkonen J, Örmälä T, Holmberg C. 2006a. Long-term clinical outcome in patients with congenital chloride diarrhea. *J Pediatr Gastroenterol Nutr*.

Hihnala S, Kujala M, Toppari J, Kere J, Holmberg C, Höglund P. 2006b. Expression of SLC26A3, CFTR and NHE3 in the human male reproductive tract: role in male subfertility caused by congenital chloride diarrhoea. *Mol Hum Reprod*.

Höglund P, Hihnala S, Kujala M, Tiitinen A, Dunkel L, Holmberg C. 2006. Disruption of the SLC26A3-mediated anion transport is associated with male subfertility. *Fertil Steril*.

Hwang JY, Mannowetz N, Zhang Y, Everley RA, Gygi SP, Bewersdorf J, Lishko P V., Chung JJ. 2019. Dual sensing of physiologic pH and calcium by EFCAB9 regulates sperm motility. *Cell*.

Jansen V, Alvarez L, Balbach M, Strünker T, Hegemann P, Kaupp UB, Wachten D. 2015. Controlling fertilization and cAMP signaling in sperm by optogenetics. *Elife*.

Kaupp UB, Strünker T. 2017. Signaling in sperm: more different than similar. *Trends Cell Biol*.

Khalifah RG, Silverman DN. 1991. Carbonic anhydrases kinetics and molecular function. In: Dogson SJ, Tashian RE, Gros G, Carter ND, editors. The Carbonic Anhydrases. Cellular Physiology and Molecular Genetics.

Kirichok Y, Navarro B, Clapham DE. 2006. Whole-cell patch-clamp measurements of spermatozoa reveal an alkaline-activated Ca^{2+} channel. *Nature*.

Lamy CM, Chatton JY. 2011. Optical probing of sodium dynamics in neurons and astrocytes. *Neuroimage*.

Leclerc P, De Lamirande E, Gagnon C. 1996. Cyclic adenosine 3',5'monophosphate-dependent regulation of protein tyrosine phosphorylation in relation to human sperm capacitation and motility. *Biol Reprod*.

Levine N, Marsh DJ. 1971. Micropuncture studies of the electrchemical aspects of fluid and electrolyte transport in individual seminoferous tubules, the epididymis and the vas deferens in rats. *J Physiol*.

Li CY, Jiang LY, Chen WY, Li K, Sheng HQ, Ni Y, Lu JX, Xu WX, Zhang SY, Shi QX. 2010. CFTR is essential for sperm fertilizing capacity and is correlated with sperm quality in humans. *Hum Reprod*.

Linares-Hernández L, Guzmán-Grenfell AM, Hicks-Gomez JJ, González-Martínez MT. 1998. Voltage-dependent calcium influx in human sperm assessed by simultaneous optical detection of intracellular calcium and membrane potential. *Biochim Biophys Acta - Biomembr*.

Lishko P V., Botchkina IL, Fedorenko A, Kirichok Y. 2010. Acid extrusion from human spermatozoa is mediated by flagellar voltage-gated proton channel. *Cell*.

Lishko P V., Botchkina IL, Kirichok Y. 2011. Progesterone activates the principal Ca^{2+} channel of human sperm. *Nature*.

López-González I, Torres-Rodríguez P, Sánchez-Carranza O, Solís-López A, Santi CM, Darszon A, Treviño CL. 2014. Membrane hyperpolarization during human sperm capacitation. *Mol Hum Reprod*.

Lu J, Stewart AJ, Sadler PJ, Pinheiro TJT, Blindauer CA. 2008. Albumin as a zinc carrier: properties of its high-affinity zinc-binding site. *Biochem Soc Trans*.

Maas DHA, Storey BT, Mastroianni L. 1977. Hydrogen ion and carbon dioxide content of the oviductal fluid of the rhesus monkey (Macaca mulatta). *Fertil Steril*.

MacDonald RR, Lumley IB. 1970. Endocervical pH measured in vivo through the normal menstrual cycle. *Obstet Gynecol*.

Mall MA, Hartl D. 2014. CFTR: Cystic fibrosis and beyond. *Eur Respir J*.

Matsuoka R, Fudim R, Jung S, Zhang C, Bazzone A, Chatzikyriakidou Y, Robinson C V., Nomura N, Iwata S, Landreh M, Orellana L, Beckstein O, Drew D. 2022. Structure, mechanism and lipid-mediated remodeling of the mammalian Na^+/H^+ exchanger NHA2. *Nat Struct Mol Biol*.

Meizel S, Deamer DW. 1978. The pH of the hamster sperm acrosome. *J Histochem Cytochem*.

Miller MR, Kenny SJ, Mannowetz N, Mansell SA, Wojcik M, Mendoza S, Zucker RS, Xu K, Lishko P V. 2018. Asymmetrically Positioned Flagellar Control Units Regulate Human Sperm Rotation. *Cell Rep*.

Mukherjee S, Jansen V, Jikeli JF, Hamzeh H, Alvarez L, Dombrowski M, Balbach M, Strünker T, Seifert R, Kaupp UB, Wachten D. 2016. A novel biosensor to study cAMP dynamics in cilia and flagella. *Elife*.

Müller F, Aschenbach JR, Gäbel G. 2000. Role of Na^+/H^+ exchange and HCO_3^- transport in pH_i recovery from intracellular acid load in cultured epithelial cells of sheep rumen. *J Comp Physiol - B Biochem Syst Environ Physiol*.

Musset B, Capasso M, Cherny V V., Morgan D, Bhamrah M, Dyer MJS, DeCoursey TE. 2010. Identification of Thr29 as a critical phosphorylation site that activates the human proton channel Hvcn1 in leukocytes. *J Biol Chem*.

Nakanishi T, Ikawa M, Yamada S, Toshimori K, Okabe M. 2001. Alkalinization of acrosome measured by GFP as a pH indicator and its relation to sperm capacitation. *Dev Biol*.

Navarro B, Kirichok Y, Clapham DE. 2007. KSper, a pH-sensitive K^+ current that controls sperm membrane potential. *Proc Natl Acad Sci U S A*.

Ng KYB, Mingels R, Morgan H, Macklon N, Cheong Y. 2018. In vivo oxygen, temperature and pH dynamics in the female reproductive tract and their importance in human conception: A systematic review. *Hum Reprod Update*.

Nishigaki T, Wood CD, Shiba K, Baba SA, Darszon A. 2006. Stroboscopic illumination using light-emitting diodes reduces phototoxicity in fluorescence cell imaging. *Biotechniques*.

Orta G, De La Vega-Beltran JL, Martín-Hidalgo XD, Santi CM, Visconti PE, Darszon XA. 2018. CatSper channels are regulated by protein kinase A. *J Biol Chem*.

Owen DH, Katz DF. 2005. A review of the physical and chemical properties of human semen and the formulation of a semen simulant. *J Androl*.

Owen DH, Katz DF. 1999. A vaginal fluid simulant. *Contraception*.

Parker MD, Ourmozdi EP, Tanner MJA. 2001. Human BTR1, a new bicarbonate transporter superfamily member and human AE4 from kidney. *Biochem Biophys Res Commun*.

Parkkila S, Rajaniemi H, Kellokumpu S. 1993. Polarized expression of a band 3-related protein in mammalian sperm cells. *Biol Reprod*.

Parrish JJ, Susko-Parrish JL, First NL. 1989. Capacitation of bovine sperm by heparin: Inhibitory effect of glucose and role of intracellular pH. *Biol Reprod*.

Patrat C, Serres C, Jouannet P. 2002. Progesterone Induces Hyperpolarization after a Transient Depolarization Phase in Human Spermatozoa. *Biol Reprod*.

Pedersen SF, Counillon L. 2019. The SLC9A-C mammalian Na^+/H^+ exchanger family: molecules, mechanisms, and physiology. *Physiol Rev*.

Puga Molina LC, Luque GM, Balestrini PA, Marín-Briggiler CI, Romarowski A, Buffone MG. 2018a. Molecular basis of human sperm capacitation. *Front Cell Dev Biol*.

Puga Molina LC, Pinto NA, Torres NI, González-Cota AL, Luque GM, Balestrini PA, Romarowski A, Krapf D, Santi CM, Treviño CL, Darszon A, Buffone MG. 2018b. CFTR/ENaC-dependent regulation of membrane potential during human sperm capacitation is initiated by bicarbonate uptake through NBC. *J Biol Chem*.

Puga Molina LC, Pinto NA, Torres Rodríguez P, Romarowski A, Vicens Sanchez A, Visconti PE, Darszon A, Treviño CL, Buffone MG. 2017. Essential role of CFTR in PKA-dependent phosphorylation, alkalinization, and hyperpolarization during human sperm capacitation. *J Cell Physiol*.

Raffi RO, Moghissi KS, Sacco AG. 1977. Proteins of human vaginal fluid. *Fertil Steril*.

Rahman N, Buck J, Levin LR. 2013. pH sensing via bicarbonate-regulated "soluble" adenylyl cyclase (sAC). *Front Physiol*.

Ramsey IS, Moran MM, Chong JA, Clapham DE. 2006. A voltage-gated proton-selective channel lacking the pore domain. *Nature*.

Ren D, Navarro B, Perez G, Jackson AC, Hsu S, Shi Q, Tilly JL, Clapham DE. 2001. A sperm ion channel required for sperm motility and male fertility. *Nature*.

Rennhack A, Schiffer C, Brenker C, Fridman D, Nitao ET, Cheng YM, Tamburrino L, Balbach M, Stölting G, Berger TK, Kierzek M, Alvarez L, Wachten D, Zeng XH, Baldi E, Publicover SJ, Kaupp UB, Strünker T. 2018. A novel cross-species inhibitor to study the function of CatSper Ca^{2+} channels in sperm. *Br J Pharmacol*.

Richard Chaillet J, Boron WF. 1985. Intracellular calibration of a pH-sensitive dye in isolated, perfused salamander proximal tubules. *J Gen Physiol*.

Riffo M, Leiva S, Astudillo J. 1992. Effect of zinc on human sperm motility and the acrosome reaction. *Int J Androl*.

Rode B, Dirami T, Bakouh N, Rizk-rabin M, Norez C, Lhuillier P, Lorès P, Jollivet M, Melin P, Zvetkova I, Bienvenu T, Becq F, Planelles G, Edelman A, Gacon G, Touré A. 2012. The testis anion transporter TAT1 (SLC26A8) physically and functionally interacts with the cystic fibrosis transmembrane conductance regulator channel: a potential role during sperm capacitation. *Hum Mol Genet*.

Romero F, Nishigaki T. 2019. Comparative genomic analysis suggests that the sperm-specific sodium/proton exchanger and soluble adenylyl cyclase are key regulators of CatSper among the Metazoa. *Zool Lett*.

Romero MF, Chen AP, Parker MD, Boron WF. 2013. The SLC4 family of bicarbonate (HCO_3^-) transporters. *Mol Aspects Med*.

Sakman B, Neher E. 1984. Patch clamp techniques for studying ionic channels in excitable membranes. *Annu Rev Physiol*.

Samanta L, Parida R, Dias TR, Agarwal A. 2018. The enigmatic seminal plasma: A proteomics insight from ejaculation to fertilization. *Reprod Biol Endocrinol*.

Santi CM, Martínez-López P, de la Vega-Beltrán JL, Butler A, Alisio A, Darszon A, Salkoff L. 2010. The SLO3 sperm-specific potassium channel plays a vital role in male fertility. *FEBS Lett*.

Sasaki M, Takagi M, Okamura Y. 2006. A voltage sensor-domain protein is a voltage-gated proton channel. *Science (80-)*.

Schiffer C, Rieger S, Brenker C, Young S, Hamzeh H, Wachten D, Tüttelmann F, Röpke A, Kaupp UB, Wang T, Wagner A, Krallmann C, Kliesch S, Fallnich C, Strünker T. 2020. Rotational motion and rheotaxis of human sperm do not require functional CatSper channels and transmembrane Ca^{2+} signaling. *EMBO J*.

Schulz S, Jakubiczka S, Kropf S, Nickel I, Muschke P, Kleinstein J. 2006. Increased frequency of cystic fibrosis transmembrane conductance regulator gene mutations in infertile males. *Fertil Steril*.

Seifert R, Flick M, Bönigk W, Alvarez L, Trötschel C, Poetsch A, Müller A, Goodwin N, Pelzer P, Kashikar ND, Kremmer E, Jikeli J, Timmermann B, Kuhl H, Fridman D, Windler F, Kaupp UB, Strünker T. 2015. The CatSper channel controls chemosensation in sea urchin sperm. *EMBO J*.

Spehr M, Schwane K, Riffell JA, Barbour J, Zimmer RK, Neuhaus EM, Hatt H. 2004. Particulate adenylate cyclase plays a key role in human sperm olfactory receptor-mediated chemotaxis. *J Biol Chem*.

Strünker T, Goodwin N, Brenker C, Kashikar ND, Weyand I, Seifert R, Kaupp UB. 2011. The CatSper channel mediates progesterone-induced Ca^{2+} influx in human sperm. *Nature*.

Su YH, Vacquier VD. 2002. A flagellar K+-dependent Na^{+}/Ca^{2+} exchanger keeps Ca^{2+} low in sea urchin spermatozoa. *Proc Natl Acad Sci U S A*.

Suarez SS, Pacey AA. 2006. Sperm transport in the female reproductive tract. *Hum Reprod Update*.

Tang L, Fatehi M, Linsdell P. 2009. Mechanism of direct bicarbonate transport by the CFTR anion channel. *J Cyst Fibros*.

Tjokronegoro A, Sirisinha S. 1975. Quantitative analysis of immunoglobulins and albumin in secretion of female reproductive tract. *Fertil Steril*.

Touré A, Lhuillier P, Gossen JA, Kuil CW, Lhôte D, Jégou B, Escalier D, Gacon G. 2007. The Testis Anion Transporter 1 (Slc26a8) is required for sperm terminal differentiation and male fertility in the mouse. *Hum Mol Genet*.

Touré A, Morin L, Pineau C, Becq F, Dorseuil O, Gacon G. 2001. Tat1, a novel sulfate transporter specifically expressed in human male germ cells and potentially linked to RhoGTPase signaling. *J Biol Chem*.

Trötschel C, Hamzeh H, Alvarez L, Pascal R, Lavryk F, Bönigk W, Körschen HG, Müller A, Poetsch A, Rennhack A, Gui L, Nicastro D, Strünker T, Seifert R, Kaupp UB. 2020. Absolute proteomic quantification reveals design principles of sperm flagellar chemosensation. *EMBO J*.

Veitinger T, Riffell JR, Veitinger S, Nascimento JM, Triller A, Chandsawangbhuwana C, Schwane K, Geerts A, Wunder F, Berns MW, Neuhaus EM, Zimmer RK, Spehr M, Hatt H. 2011. Chemosensory Ca^{2+} dynamics correlate with diverse behavioral phenotypes in human sperm. *J Biol Chem*.

Visconti PE, Bailey JL, Moore GD, Pan D, Olds-Clarke P, Kopf GS. 1995. Capacitation of mouse spermatozoa. II. Protein tyrosine phosphorylation and capacitation are regulated by a cAMP-dependent pathway. *Development*.

Visconti PE, Krapf D, De La Vega-Beltrán JL, Acevedo JJ, Darszon A. 2011. Ion channels, phosphorylation and mammalian sperm capacitation. *Asian J Androl*.

Vishwakarma P. 1962. The pH and bicarbonate-ion content of the oviduct and uterine fluids. *Fertil Steril*.

Vredenburgh-Wilberg WL, Parrish JJ. 1995. Intracellular pH of bovine sperm increases during capacitation. *Mol Reprod Dev*.

Wagner G, Ottesen B. 1982. Vaginal physiology during menstruation. *Ann Intern Med*.

Wandernoth PM, Mannowetz N, Szczyrba J, Grannemann L, Wolf A, Becker HM, Sly WS, Wennemuth G. 2015. Normal fertility requires the expression of carbonic anhydrases II and IV in sperm. *J Biol Chem*.

Wandernoth PM, Raubuch M, Mannowetz N, Becker HM, Deitmer JW, Sly WS, Wennemuth G. 2010. Role of carbonic anhydrase IV in the bicarbonate-mediated activation of murine and human sperm. *PLoS One*.

Wang D, Hu J, Bobulescu IA, Quill TA, McLeroy P, Moe OW, Garbers DL. 2007. A sperm-specific Na+/H+ exchanger (sNHE) is critical for expression and in vivo bicarbonate regulation of the soluble adenylyl cyclase (sAC). *Proc Natl Acad Sci U S A*.

Wang D, King SM, Quill TA, Doolittle LK, Garbers DL. 2003. A new sperm-specific Na^+/H^+ exchanger required for sperm motility and fertility. *Nat Cell Biol*.

Wang G, Guo Y, Zhou T, Shi X, Yu J, Yang Y, Wu Y, Wang J, Liu M, Chen X, Tu W, Zeng Y, Jiang M, Li S, Zhang P, Zhou Q, Zheng B, Yu C, Zhou Z, Guo X, Sha J. 2013. In-depth proteomic analysis of the human sperm reveals complex protein compositions. *J Proteomics*.

Wang T, Young S, Krenz H, Tüttelmann F, Röpke A, Krallmann C, Kliesch S, Zeng XH, Brenker C, Strünker T. 2020. The Ca^{2+} channel CatSper is not activated by cAMP/PKA signaling but directly affected by chemicals used to probe the action of cAMP and PKA. *J Biol Chem*.

Wennemuth G, Carlson AE, Harper AJ, Babcock DF. 2003. Bicarbonate actions on flagellar and Ca^{2+}-channel responses: initial events in sperm activation. *Development*.

Windler F, Bönigk W, Körschen HG, Grahn E, Strünker T, Seifert R, Kaupp UB. 2018. The solute carrier SLC9C1 is a Na^+/H^+-exchanger gated by an S4-type voltage-sensor and cyclic-nucleotide binding. *Nat Commun*.

Xiang M, Feng M, Muend S, Rao R. 2007. A human Na^+/H^+ antiporter sharing evolutionary origins with bacterial NhaA may be a candidate gene for essential hypertension. *Proc Natl Acad Sci U S A*.

Xu WM, Shi QX, Chen WY, Zhou CX, Ni Y, Rowlands DK, Yi Liu G, Zhu H, Ma ZG, Wang XF, Chen ZH, Zhou SC, Dong HS, Zhang XH, Chung YW, Yuan YY, Yang WX, Chan HC. 2007. Cystic fibrosis transmembrane conductance regulator is vital to sperm fertilizing capacity and male fertility. *Proc Natl Acad Sci*.

Yang CF, Tsai WC. 2022. Calmodulin: The switch button of calcium signaling. *Tzu Chi Med J*.

Ye G, Chen C, Han D, Xiong X, Kong Y, Wan B, Yu L. 2006. Cloning of a novel human NHEDC1 (Na^+/H^+ exchanger like domain containing 1) gene expressed specifically in testis. *Mol Biol Rep*.

Zeng X-H, Navarro B, Xia X-M, Clapham DE, Lingle CJ. 2013. Simultaneous knockout of Slo3 and CatSper1 abolishes all alkalization- and voltage-activated current in mouse spermatozoa. *J Gen Physiol*.

Zeng Y, Clark EN, Florman HM. 1995. Sperm membrane potential: Hyperpolarization during capacitation regulates zona pellucida-dependent acrosomal secretion. *Dev Biol*.

Zeng Y, Oberdorf JA, Florman HM. 1996. pH regulation in mouse sperm: Identification of Na^+-, Cl^--, and HCO_3^--dependent and arylaminobenzoate-dependent regulatory mechanisms and characterization of their roles in sperm capacitation. *Dev Biol*.

Zhang Y, Malekpour M, Al-Madani N, Kahrizi K, Zanganeh M, Mohseni M, Mojahedi F, Daneshi A, Najmabadi H, Smith RJH. 2007. Sensorineural deafness and male infertility: A contiguous gene deletion syndrome. *J Med Genet*.

Zhao R, Dai H, Arias RJ, De Blas GA, Orta G, Pavarotti MA, Shen R, Perozo E, Mayorga LS, Darszon A, Goldstein SAN. 2021. Direct activation of the proton channel by albumin leads to human sperm capacitation and sustained release of inflammatory mediators by neutrophils. *Nat Commun*.